12-2014

Development of models for the study of the molecular mechanisms of host restriction and adaptation of hantaviruses.

Ryan Carroll McAllister 1988-
University of Louisville

DEVELOPMENT OF MODELS FOR THE STUDY OF THE MOLECULAR MECHANISMS OF HOST RESTRICTION AND ADAPTATION OF HANTAVIRUSES

By

Ryan Carroll McAllister
B.S. Biochemistry, Northern Michigan University, 2010

A Thesis
Submitted to the Faculty of the
The School of Medicine of the University of Louisville
in Partial Fulfillment of the Requirements
for the Degree of

Master of Science

Department of Pharmacology and Toxicology
University of Louisville
Louisville, Kentucky

December, 2014

DEVELOPMENT OF MODELS FOR THE STUDY OF THE MOLECULAR MECHANISMS OF HOST RESTRICTION AND ADAPTATION OF HANTAVIRUSES

By

Ryan McAllister
B.S. Biochemistry, Northern Michigan University, 2010

Thesis Approved on

October 25, 2013

By the following Thesis Committee

Colleen B. Jonsson Ph.D.

Gavin E. Arteel, Ph.D.

Igor S. Lukashevich Ph.D.

Kenneth E. Palmer Ph.D.

Susanna K. Remold Ph.D.

ACKNOWLEDGMENTS

I acknowledge Dr. Colleen Jonsson for her expertise, guidance, training, and development of myself into a professional scientist. In addition, I acknowledge the Jonsson laboratory: Dr. Yong-Kyu Chu, Jeremy Camp, Rachael Gerlach, and Scott Adcock for their training, everyday help, and support.

I thank my family (Paula, Gordon, and my brother Kyle) and friends (Justin, Danny, and Scott) for their encouragement and positive reinforcement throughout my graduate career. Most importantly I would like to acknowledge my extended family for understanding my absences and how busy I am during my graduate school process. Most importantly, I would like to acknowledge my grandfather, Paul Leon Carroll, for his guidance throughout the early portion of my life and molding me into who I am today (his passing was 11 years to the date of completing this thesis); "Don't ever give anyone a club to hit you with." Lastly, I would like to acknowledge my baby boy, Tyson, for his efforts to keep my spirit high during my graduate career, his patience to go on walks or to go play outside when I was busy with school work, and his every day fun loving attitude about life.

ABSTRACT
MOLECULAR MECHANISMS OF HOST RESTRICTION AND ADAPTATION OF HANTAVIRUSES

Ryan C. McAllister

October 25, 2013

Hantaviruses, family Bunyaviridae, are present throughout the globe in a variety of mouse, rat, mole, vole, shrew, or bat species. Hantaviruses persist for the lifetime of the animal reservoir, while causing no signs or symptoms of disease. Only the rodent-borne hantaviruses cause disease in humans. In contrast, a "spillover" infection of a hantavirus into a nonreservoir rodent species results in an asymptomatic acute infection. We and others in the field are interested in understanding the biology of these virus-host interactions and mechanisms that underlie these three very different outcomes.

The second chapter of my thesis focused on probing the intrahost viral population structure of the Hantaan virus (HTNV), an Old World hantavirus, in the suckling mouse model in the presence and absence of ribavirin. This model represents a lethal disease outcome in a nonreservoir species. These studies show, for the first time, two distinct evolutionary trajectories for HTNV within this lethal mouse model of disease in the presence and absence of ribavirin, as well as evidence for positive selection not previously observed in vitro. In the ribavirin-treated vRNA population, analyses of rates of nonsynonymous (*dN*) and

synonymous (*dS*) substitutions in the S-segment revealed a positive selection for codons within the HTNV N protein gene, while untreated, HTNV-infected mice showed purifying selection.

The third chapter of my thesis focused on development of a physiologically relevant, in vitro model of the hantavirus-rodent reservoir interaction; specifically, the deer mouse (*Peromyscus maniculatus*) and Sin Nombre virus. As the primary target of hantaviral infection is the vascular endothelium, a primary lung microvascular endothelial cell (L-MVEC) culture system was established. Culture conditions were established and optimized for passage and infection. Future research will use this model to probe viral determinants and mechanisms that promote persistence and identify host responses that pose barriers to virus adaptation.

TABLE OF CONTENTS

ACKNOWLEDGEMENTS	.....	iii
ABSTRACT	.....	iv
LIST OF TABLES	.....	viii
LIST OF FIGURES	.....	ix
CHAPTER I	HANTAVIRUSES PAST, PRESENT, AND FUTURE ...	1
	An introduction to the discovery of hantaviruses and their diseases	1
	Coding and replication strategy of the *Hantavirus* genome	3
	Structure and function of hantaviral proteins	4
	Differential immune responses in rodents and humans	9
	Hantaviral mechanisms in regulation of nonreservoir host immune responses	15
	Conclusion	20
	Future perspective for treatment	22
CHAPTER II	THE MURINE MODEL FOR HANTAAN VIRUS-INDUCED LETHAL DISEASE SHOWS TWO DISTINCT PATHS IN VIRAL EVOLUTIONARY TRAJECTORY WITH OR WITHOUT RIBAVIRIN TREATMENT	24
	Introduction	24
	Mechanisms of viral evolution	25
	Tools for the evaluation of genetic changes in viral genomes	28
	In vivo modes of hantaviral infection	31
	Materials and Methods	34
	Cells and virus	34
	Animal study	34
	Isolation of total RNA, cDNA synthesis, and RT-PCR	35
	Sequencing and phylogenetic analysis	36
	Ratio of nonsynonymous to synonymous substitution rates	37
	Statistical analysis	37
	Results	38
	Study design	38
	Viral titers in lungs in mock- and	41

	ribavirin treated mice		
	Intrahost genetic variation of HTNV in untreated and ribavirin-treated mice	.....	45
	Phylogenetic relationships of sequences	.....	53
	Ratio of nonsynonymous to synonymous substitution rates	.....	55
	Discussion	.....	59
CHAPTER III	A NEW PRIMARY LUNG MICROVASCULAR ENDOTHELIAL CELL CULTURE MODEL FROM DEER MOUSE TO STUDY NEW WORLD HANTAVIRUS INFECTIONS	.....	66
	Introduction	.....	66
	Materials and Methods	.....	70
	Viruses and deer mice	.....	70
	Isolation and culture of lung microvascular endothelial cells (L-MVEC) from deer mice	.....	70
	FACS analyses	.....	73
	Infections and treatment of L-MVEC	.....	73
	Western blots	.....	74
	Plaque Assay	.....	75
	Virus cell-based ELISA	.....	75
	Relative expression levels of cytokines, chemokines and quantification of viral RNA by qRT-PCR	.....	76
	Results	.....	78
	Isolation and culture of deer mouse L-MVEC	.....	78
	Characterization of L-MVEC	.....	79
	Permissiveness of deer mouse L-MVEC to hantaviral infection	.....	83
	Innate immune signaling profiles mounted by deer mouse L-MVEC when infected with reservoir and nonreservoir hantaviruses	.....	90
	Discussion	.....	93
	Future Studies	.....	97
	Conclusion	.....	100
REFERNCES	.....		103
APPENDIX	.....		114
CURRICULUM VITA	.....		116

LIST OF TABLES

Table	Title	Page
1	Datamonkey analysis for determining selection	30
2	Group, treatment and sampling design	40
3	Summary of mock and ribavirin-treated, HTNV-infected mutation frequencies	47
4	Amino acid changes within HNTV S-segment in mice	51
5	Summary of MEME, IFEL and FUBAR analyses	58
6	Primers to assess cytokine and chemokine expression levels	77
7	Cell-based ELISA and plaque assay titers of infected deer mouse L-MVEC at MOI's of 1.0 and 0.06, 48 hpi and Vero E6 seed stock viruses	89
8	L-MVEC characterization approach for FACS or Western Blot/Microscopy	95
9	Proposed viruses and predicted phenotypes	102

LIST OF FIGURES

Figure	Title	Page
1	Hantavirus life cycle	6
2	Cellular players and responses in rodent reservoir and human infections with hantaviruses	13
3	Molecular interactions of N protein	17
4	Viral RNA and infectious virus levels in lung tissue of untreated and ribavirin-treated, HTNV-infected mice.	43
5	Average intrahost genetic variability of HTNV population in mock- and ribavirin-treated mice.	48
6	Selective infectivity of animals from untreated and ribavirin-treated animals	49
7	Illustration summarizing the locations of amino acid changes in the HTNV N protein.	52
8	Maximum likelihood phylogeny of the open reading frame of the S-segment and wild type HNTV sequences	54
9	Outline of method for isolation of L-MVEC	72
10	Deer mouse isolated L-MVEC	81
11	FACS analysis of deer mouse L-MVEC	82
12	Viral replication of SNV S-segment in infected deer mouse L-MVEC	87
13	Deer mouse infected L-MVEC western blot analysis	88
14	Infected deer mouse L-MVEC innate immune signaling	92

CHAPTER I

HANTAVIRUSES PAST, PRESENT, AND FUTURE

An introduction to the discovery of hantaviruses and their diseases

Historical retrospectives of medical reports suggest trench nephritis in the first World War, nephropathia epidemica (NE) in Scandinavia, Song-go fever in Manchuria and hemorrhagic nephroso-nephritis in the Soviet Union were all potentially caused by hantaviruses [1-4]. However, it was not until Hantaan virus (HTNV) was isolated in 1977 that two human diseases were attributed to hantaviruses; hemorrhagic fever with renal syndrome (HFRS) in Europe and Asia, and NE, a mild form of HFRS, in northern Europe. Four *Hantavirus* species are now recognized to cause HFRS (HTNV harbored by *Apodemus agrarius* [1]; Dobrava-Belgrade virus (DOBV) is harbored by *A. agrarius. A flavicollis*, and *A. ponticus* rodents [5, 6]; Seoul virus (SEOV) is harbored by *Rattus norvegicus* [7]) and NE (Puumala virus, PUUV, harbored by *Myodes glareolus*). Combined these viruses have a global public health impact estimated at over 50,000 cases each year with lethality ranging from 1 to 12% [8].

The wide prevalence of hantaviruses in rodents in Europe and Asia suggested they could be potential reservoirs for hantaviruses in the Americas. In the mid-1980's rodent surveillance efforts discovered Prospect Hill virus (PHV) harbored by *Microtus pennyslvanicus* [9], and cross reactive antibodies were

reported in *Peromyscus maniculatus, P. difficilis, P. californicus, Neotoma mexicana, N. cinerea* [10] in the USA, and in Old World (laboratory) rodents in South America [11]. It was not long after these efforts that an outbreak of hantavirus pulmonary syndrome (HPS) in persons residing in the Four Corners area in the southwestern USA in 1993 confirmed the presence of disease causing hantaviruses in the Americas.

In the Spring of 1993, two young, healthy adults living in the Navajo Nation fell ill and died from an unexplained adult respiratory distress syndrome (ARDS) [12]. Unexplained deaths are reported to the Office of the Medical Investigator (OMI) in New Mexico. Discussions between the OMI and the Indian Health Service quickly recognized there were at least five cases of ARDS in the region. The outbreak led to collaborative investigations by state health departments in Arizona, Colorado, New Mexico, and Utah; the Indian Health Service; the OMI, the University of New Mexico, and the Center for Disease Control (CDC), with the assistance of the Navajo Nation Division of Health to identify cases, rodent reservoirs and develop diagnostic and treatment approaches. Within a year's time, the CDC identified the causative agent as Sin Nombre virus (SNV) harbored by *Peromyscus maniculatus* [13], a New World rodent species, and one of the rodents reported having antibodies to hantaviral antigens in 1985 [10]. Other groups also reported the identification of SNV [14] and SN-like viruses from patients and a number of other rodent reservoirs [8, 15].

Just two years after the outbreak in the USA, outbreaks of HPS were recognized in Argentina and Chile caused by Andes virus (ANDV) [16-18], and in

Paraguay caused by Laguna Negra virus (LANV) [19, 20]. In Paraguay, the outbreak was associated with those living in the agricultural communities within the Chaco. In contrast to the severity of disease and high mortality (50%) caused by ANDV, the disease caused by LANV shows a lower mortality (<15%) [21]. In the third outbreak in El Bolson, Argentina in 1996 [22], one physician in Buenos Aires fell ill 27 days after taking care of an HPS patient from El Bolson [23]. This was the first recognition that these viruses may cause person to person transmission of the illness. Since that report, additional studies have shown that person-to-person transmission can occur between couples, persons who sleep in the same bed or room of index patients with ANDV infection, or sustained contact during travel (e.g., on a bus) [23-26].

Coding and replication strategy of the *Hantavirus* genome

Hantaviruses, family Bunyaviridae, are negative-sense, single-stranded RNA viruses with three gene segments (or viral RNAs, vRNAs): small (S), medium (M) and large (L) [27]. The S-segment encodes for the nucleocapsid (N) protein, the M-segment encodes for the G_N and G_C glycoproteins, and the L-segment encodes for the RNA dependent RNA polymerase (RdRp). In the S-segment of the hantaviruses carried by *Arvicolinae* and *Sigmodontinae*, but not *Muridae* rodents, the N protein has an overlapping (+1) open reading frame for a small, nonstructural protein (NSs) [28, 29]. The ends of each segment of the genome have conserved, inverted, complementary 5' and 3' termini structure that can form a panhandle [30, 31], which has been shown with other viruses in the

Bunyaviridae [32, 33]. This region of the genome may contain *cis*-acting elements that promote replication of the viral RNA (vRNA), complementary RNAs (cRNAs) and messenger RNA (mRNA) transcription by the RdRp [30, 31]. The N protein packages each of the three vRNA into three ribonucleoprotein (RNP) complexes which are contained within the virus [8]. By cryoelectron microscopy (Cryo-EM), the virion contains three to four rod-like RNP structures [34, 35], which presumably contain each vRNA wrapped in N proteins. The viral polymerase would be expected to be part of the RNP.

Reverse genetic approaches have been successful for other members of the Bunyaviridae [36-39], but success in applying these strategies to hantaviruses has been limited [40]. At present there has been no progress in the creation of systems for the generation of infectious, recombinant hantaviruses. The challenges in generating recombinant systems for the study of hantaviruses may be due to the ability to produce the correct structures of the tripartite genomes, which have a 5-prime monophosphate [41] or additional unknown structural features.

Structure and function of hantaviral proteins

Hantavirus virions are asymmetric, pleomorphic particles, and until recently were thought to have an average diameter of approximately 80-120 nm [8, 42]. Electron microscopy studies of the HTNV and Tula virus (TULV) virions now show the particles range in size from 120-154 nm [34, 35]. The surface rendering of the virion suggests an unusual square, grid-like pattern distinct from

other genera in the *Bunyaviridae* and a lack of icosahedral symmetry typical of most viruses. The square spike on the outer surface reflects the glycoprotein projections, which extend from 0 to 12 nm from the lipid bilayer and comprise 4 molecules of G_N and G_C [34].

Hantaviruses bind epithelial and endothelial cells via interaction of G_N with the host's cell surface receptor(s); β1 integrin for apathogenic and β3 integrin for pathogenic hantaviruses (**Figure 1, step A**) [43, 44]; although additional receptors or co-receptors may also promote entry such as the decay-accelerating factor (DAF/CD55) and the globular head domain of complement Clq [45]. In addition, hantaviruses infect macrophages, follicular dendritic cells, and lymphocytes [45-49]. In Vero E6 cells, HTNV has been shown to enter through clathrin coated pits and traffic to late endosomes (**Figure 1, step B**) [50]. ANDV do not enter via clathrin; the pathway for entry is not known [51]. Further, early entry events are distinct for HTNV and ANDV given their difference in the dependence on an intact actin (ANDV) versus microtubule (HTNV) cytoskeleton for viral replication [51]. Release of the RNP's into the host cell cytoplasm from endosomal compartments is pH dependent [50].

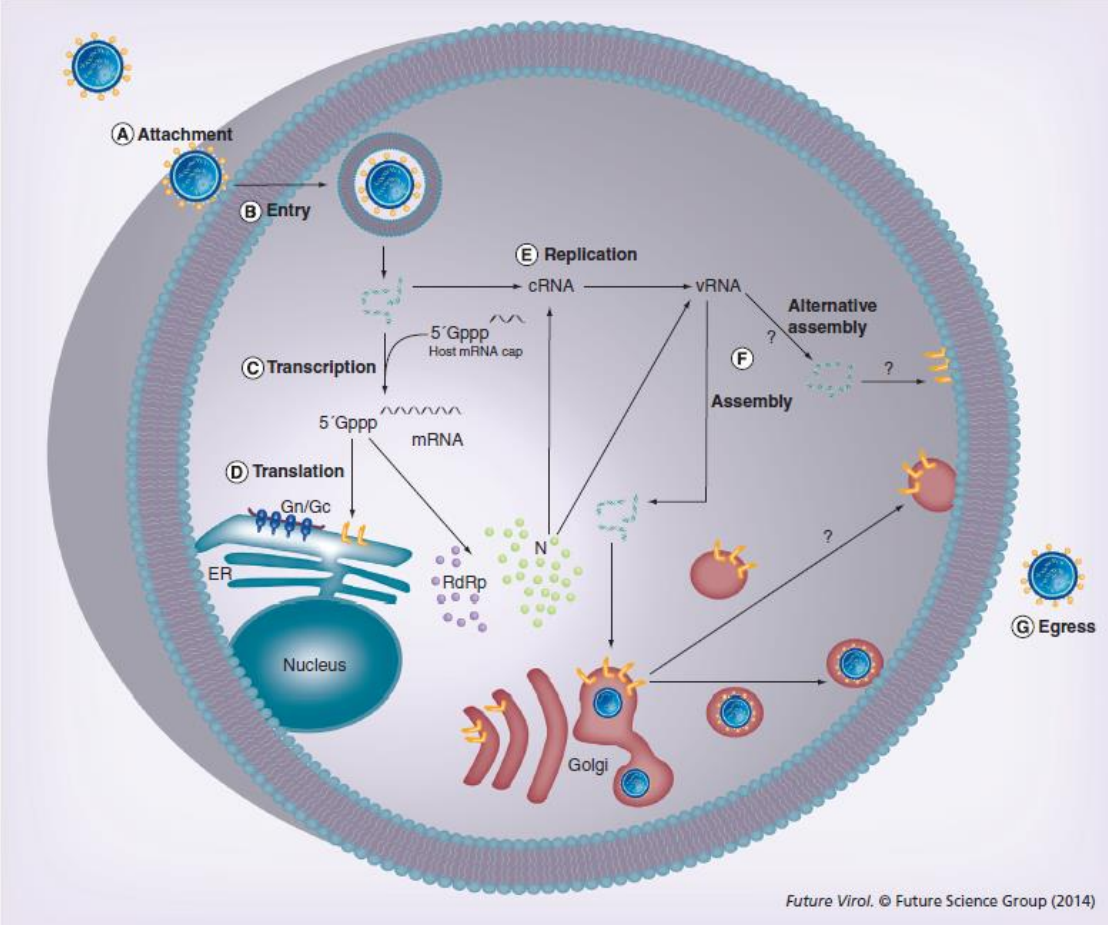

Figure 1. **Hantavirus life cycle**. The virus life cycle includes: (**A**) Attachment to either β1 or β3 integrin of the host cell surface using the viral G_N protein; (**B**) Entry of the virus through clathrin receptor mediated endocytosis; (**C**) Transcription via the RdRp cleaves host cell mRNA caps as primers for the vRNA; (**D**) Translation of the N and RdRp proteins on free ribosomes and M-segment through rough ER; (**E**) Replication of vRNA requires N protein to form the RNP; (**F**) Assembly of the virion at the Golgi or possibly for New World at the plasma membrane; (**G**) Egress from the Golgi through the plasma membrane. Reproduced from Future Virology. (2014) 9(1), 87-99 with permission of Future Medicine Ltd.

Homology modeling first suggested that the G_C has a structure similar to the alphavirus E1, which like G_C, harbors the fusion domain [52]. The alphavirus E1 is a class II fusion protein that forms a pH dependent, trimeric configuration to mediate fusion with the host cell membrane within endosomes. A class II fusion peptide maps to the G_C protein, and has been shown to promote fusion using ANDV G_N/G_C-pseudotyped lentiviral particles [52, 53]. With the recent Cryo-EM of HTNV and TULV, elucidation of the structure of the glycoproteins and mapping them within the Cryo-EM structures will shed light on how these G_N/G_C proteins change conformationally to promote membrane fusion.

While the precise site(s) for viral transcription and replication are not known, the RdRp protein transcribes viral mRNAs from each vRNA in the cytoplasm using primers derived from host cellular mRNAs (**Figure 1, step C**) [54]. The RdRp catalyzes the endonucleolytic cleavage of host cell mRNA at 7-18 nucleotides downstream from the 5' cap, this activity is also termed "cap snatching" [54]. This results in hantaviral mRNAs with heterogeneous 5'-ends, which are not polyadenylated. Translation of the S and L mRNAs occurs on free ribosomes resulting in the production of the N and RdRp proteins; and NSs in some hantaviruses (**Figure 1, step D**). The N protein, which accumulates in the perinuclear region, is the most abundant viral protein synthesized early in infection. N plays structural and functional roles in the virus life cycle including modulation of host responses, binding to vRNA, cRNA and host mRNA caps, translation initiation and assembly [31]. The timing and location at which N protein apparently commanders the host mRNA caps is not known, but the N has

been proposed to retain the caps in P bodies [55]. How these complexes traffic from the P body to the replication complex(es) is not known. While not much is yet known about the NSs, the TULV NSs localizes within the perinuclear region [56]. It is highly likely that different oligomeric states or conformations of N occur during the life cycle as demonstrated by their ability to form trimeric structures [57, 58]. While not much is yet known about the NSs, the TULV NSs have been reported to localize within the perinuclear region [56].The M-segment is cotranslated into the rough endoplasmic reticulum (RER) (**Figure 1, step D**). Following translation into the ER, the precursor protein is proteolytically cleaved at a WAASA conserved amino acid motif located from amino acids, 264-268, into G_N and G_C. A small portion of the c-terminus of the G_N extends into the cytoplasm (referred to as the G_N tail). The G_N and G_C proteins are glycosylated in the RER and translocate though the Golgi complex until they assemble into particles. The G_N cytoplasmic tail has been shown to bind to nucleic acid [59] and N protein [60]. At some point following mRNA transcription, the RdRp begins replication of the cRNAs and vRNAs (**Figure 1, step E**). The signals that initiate replication are not known, however, it has been suggested that some level of N protein in the cell could drive the switch. The N protein traffics by microtubule dynein to the ER-Golgi Intermediate Complex (ERGIC) where they may begin to complex with newly synthesized vRNAs to form RNPs [61].

It is unclear where or how the assembly of the RNP takes place, however, at least in the case of the Old World hantaviruses, the RNPs must traffic to the Golgi since this is the compartment where G_N and G_C glycoproteins are directed

and virions have been visualized (**Figure 1, step F**) [62]. The RNP may interact with the G_N cytoplasmic tail [60] and buds into the Golgi to produce the virion. A Golgi vesicle forms around newly formed particles and transports the virion to be released from the host cell plasma membrane. Alternatively, for the New World hantaviruses, it has been suggested that assembly could also take place at the host cell plasma membrane (**Figure 1, step F**). This prediction was initially based on the absence of virions within the Golgi for SNV and Black Creek Canal viruses (BCCV). There is still limited evidence for where assembly takes place, however, the glycoproteins of BCCV have been shown to be expressed at the plasma membrane on the apical surface of polarized Vero C1008 cells [63]. Further, studies by Rowe *et al*., have shown that the ANDV associates with the recycling endosome and the Rab 9/11 proteins and this may serve as an important pathway for trafficking from the Golgi to the plasma membrane [64].

Differential immune responses in rodents and humans

The survival of hantaviruses in nature depends on maintenance of persistent infections within its specific rodent reservoir. Hantaviruses infect and persist only in the rodent reservoir in which the virus has coevolved (monitored through phylogenetic trees using sequences from reservoir host mitochondria compared to hantavirus S-segment), and the infection is believed to last the life of the animal [65]. Notably, persistent infection of rodent reservoirs by hantaviruses show continuous virus replication, without complete clearance by the immune system, and no pathological changes [8]. Humans are not a natural

reservoir and therefore only become infected when they come into contact with excreta from the rodent reservoir. In humans, infection can result in severe disease although outcomes vary with different hantaviral species. There are also a number of hantaviruses that do not appear to replicate in human endothelial cells (PHV) [66] and/or cause disease in humans (TULV and PHV). The molecular basis for this has been attributed to difference in receptor preferences of apathogenic and pathogenic hantaviruses, which will be discussed later.

The clinical course and pathology of HFRS and HPS has been the subject of several excellent recent reviews [67, 68]. It is recognized that both HFRS- and HPS-causing hantaviruses cause systemic vascular leakage without apparent damage to the endothelial cells even though the target organs for HFRS and HPS differ, kidneys and lungs, respectively. In severe cases, this can lead to hypotension and shock. Mechanisms proposed for the increase in capillary leakage include infection-induced increase in vascular endothelial growth factor (VEGF), and immunopathology (indirect through cytokines released by T cells). It has been hypothesized that the immune response to hantavirus infection in human cases causes the severe disease symptoms (e.g., acute thrombocytopenia, increased leukocytes) [69]. A recent study reports a third mechanism for promotion of vascular leakage and disease. Using a novel *in vitro* capillary blood vessel model, HTNV or ANDV infection increases bradykinin (BK) through activation of the kallikrein-kinin system, which correlates with an increase in endothelial cell permeability [70]. The capillary blood vessel model cocultured human umbilical vein endothelial cells with human mesenchymal stem cells or

human pulmonary artery smooth muscle cells, which generate blood vessel like capillary structures. BK is an inflammatory peptide that can cause vasodilation and vascular permeability in the vasculature upon binding of its receptor. Interestingly, the model showed an increase in VEGF following infection, but no loss in vascular integrity. The immune responses in humans following infection with HPS and HFRS-causing viruses have been extensively reviewed [67, 69, 71-75]; therefore, in the following, we will highlight those responses that distinguish between infections of the rodent reservoir and humans.

In *Hantavirus* infection, the differences in immune responses between reservoir and humans are evident in composition, magnitude and kinetics of cytokine/chemokine responses and T cells. Generally, longitudinal studies of hantaviral infection show elevated TNF-α, IL-6, IL-2, IL-1 IL-10 IL-12 and cytotoxic T lymphocytes (CTL) responses (**Figure 2**) [76-80]. Levels of secreted cytokines and chemokines in deer mice infected with SNV cannot be compared directly, as many antibodies are not yet available. However, longitudinal studies of RNA levels of key cytokines and chemokines in lung and spleen have been reported in SNV infected deer mice [81] and SEOV-infected rats [82]. While most responses noted in humans were very low in SNV-infected deer mice (<twofold above uninfected mice) and variable, IL-12 rose at 7 days post infection (dpi) in the spleen. In addition, immune responses included increased GM-CSF (10 dpi) and TGF-β (biphasic peaks at 5 and 15 dpi) in the spleen. The lack on inflammatory signals was similar in SEOV infected rats; however, TGF-β was elevated in the lungs, not spleen [82].

Patients with severe HPS or HFRS/NE show strong CD8+T cell responses with high levels of perforin and granzyme B [79, 80]. From these studies it has been hypothesized that the strong CD8+ T-cell responses will eliminate virus, but that such intensive T-cell responses might also result in an excessive amount of cytokines, which promote capillary leakage and endothelial cell dysfunction [69, 73]. In contrast to these findings, a recent study of HFRS patients shows that the prevalence of N-antigen-specific CD8+ T cells correlated with the early, acute stages of infection and declined thereafter [83]. Hence, the CD8+T cells would be expected to have a protective effect rather than promote immune pathology. In support of these findings, T-cell-deficient Rowett nude rats infected with SEOV succumb rapidly to infection and disease, suggesting that cell-mediated immunity may play an important role in controlling infection [84]. More recently, the depletion of T cells from hamsters did not alter the progression of HPS following ANDV challenge, which suggests that vascular permeability does not involve T-cell-mediated immunopathology [85]. In summary, the present literature reports a role for CTLs in promoting disease or protection; hence a more comprehensive analysis of the CTL response is needed in many more patients. However, these studies may be confounded in that most of the hantavirus-specific CTLs may be present in organs and not accounted for during analyses of CTLs from peripheral blood mononuclear cells (PBMC). An additional complexity is in the recent finding that endothelial cells infected *in vitro* with ANDV and HTNV are protected from CTL- and NK-cell-mediated apoptosis [86].

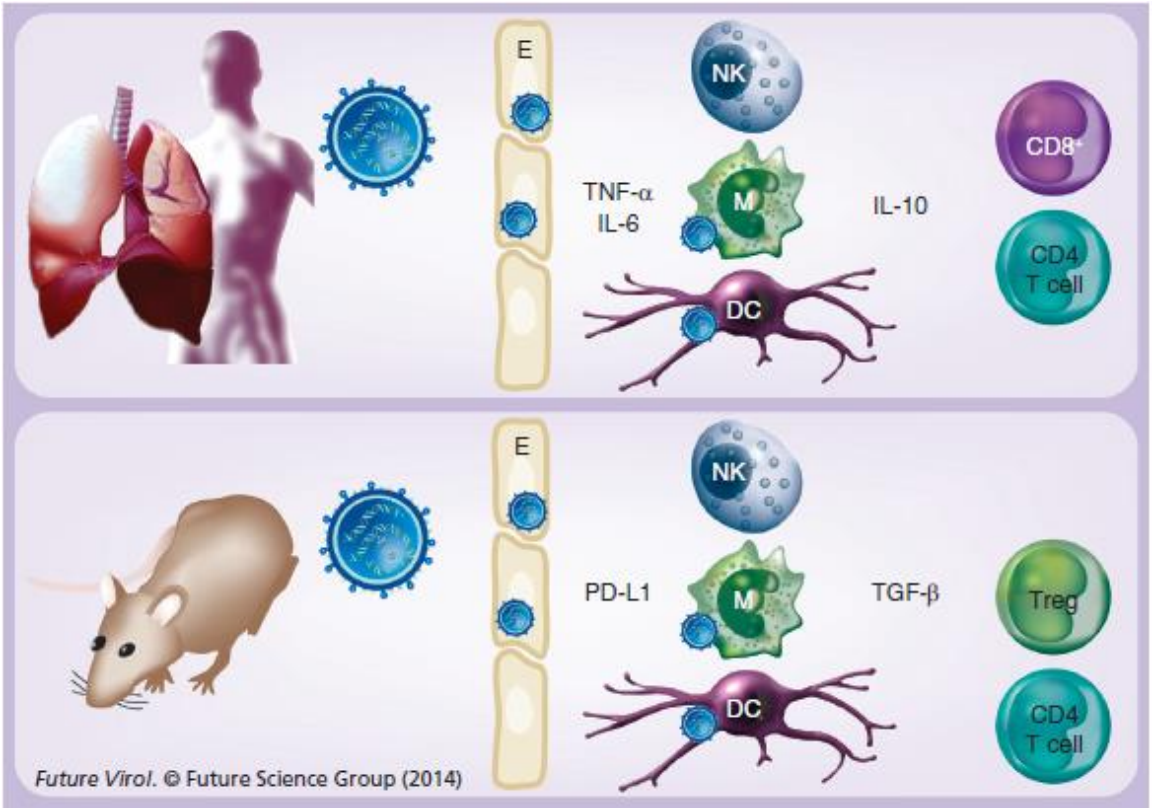

Figure 2. **Cellular players and responses in rodent reservoir and human infections with hantaviruses**. While there are many gaps in our understanding of the role of the key immune cells and their function, recent studies suggest several key immune responses. During a persistent infection reservoir species have up regulated Protein Dependent Ligand 1 (PD-L1) and TGFβ resulting regulatory T cells (Treg) response, which results in suppressed immune state. IgG antibodies are produced suggesting a CD^+4 T cell response. Whereas in humans, pro-inflammatory cytokines such as TNFα, IL6, and IL10 are induced as well as CD^+8 and CD^+4 T cells. Reproduced from Future Virology. (2014) 9(1), 87-99 with permission of Future Medicine Ltd.

Mouse models of transient and persistent infection for HTNV have been used to analyze the immune response of virus-specific $CD8^+$ T cells with major histocompatibility complex (MHC) tetramers [87, 88]. In persistently-infected mice, N-specific CTLs are strongly regulated and were suppressed in the model by an unknown mechanism [88]. Viral replication in immune cells such as monocytes, macrophages or T cells can interfere with or actively suppress immunity and cause persistence. Hence Taruishi et al, 2007 proposed that the infection of the spleen early in infection may result in infection of immune cells that suppress this response. In their persistent animal model experiments, the infection of the spleen correlates with changes in CTL responses. Consequently, due to the down-regulation of the CTLs, some of the endothelial cells may remain infected, resulting in a persistent infection in the natural reservoir.

Studies of persistent infection of SEOV in the rat [89, 90] and SNV in the deer mouse [91] suggest a role for regulatory T cells, Treg, in establishing persistence. The Treg cells are Forkhead box (Fox) $P3^+CD4^+CD25^+$ and are activated during infection of the reservoir. In contrast, these cells are reduced in HFRS patients [92], although they show no chang in PUUV-infected HFRS patients [92]. The Treg responses can enable a persistent infection by limiting T helper cell responses (T_H1, T_H2-cell) indirectly by modulating antigen-presenting cell (APC) function or directly by cell–cell contact. The production of anti-inflammatory cytokines (e.g., TGF-β and IL-10) by Treg can suppress innate immunity and pro-inflammatory responses, and thereby interfere with viral clearance and pathology [93]. Interestingly, in human cases of HFRS, higher IL-

10 correlated with higher viral load [78]. In rat macrophages infected with SEOV, nuclear factor-kappaB (NFkB)-mediated inflammatory responses noted in patients (TNF-α, IL-6, and IL-10) are suppressed [82, 94]. Interestingly, SEOV induces PD-L1 expression in rat endothelial cells and TGF-β in alveolar macrophages [49] (**Figure 1**). The PD-1-PD-L1 pathway has been correlated with increased Treg activity and also shown to play an important role in other chronic viral infections such as Human Immunodeficiency virus (HIV), Hepatitis B virus (HBV), Hepatitis C virus (HCV) and lower respiratory infections [95-97].

Hantaviral mechanisms in regulation of nonreservoir host immune responses

While gaps remain in our understanding of how hantaviruses regulate the immune responses at the molecular level, studies have suggested that viral N (**Figure 3**) and glycoproteins may interact with host cellular proteins to modulate the innate immune signaling. While gaps remain in our understanding of how hantaviruses regulate the immune responses at the molecular level, studies have suggested that viral N and glycoproteins interact with host cellular proteins to modulate the innate immune signaling (**Figure 3**). Four different cellular pathways have been implicated as targets of hantaviral antagonism in primate or human cell models of infection; IFN-α/β responses (see reviews [71, 98, 99]), JAK/STAT, TNF-α receptor-mediated signaling, and apoptosis [100]. Highlights of what are currently known regarding hantaviral N, N proteins s and/or

glycoproteins (GPCs) in modulation of these cellular activities will be summarized in the following.

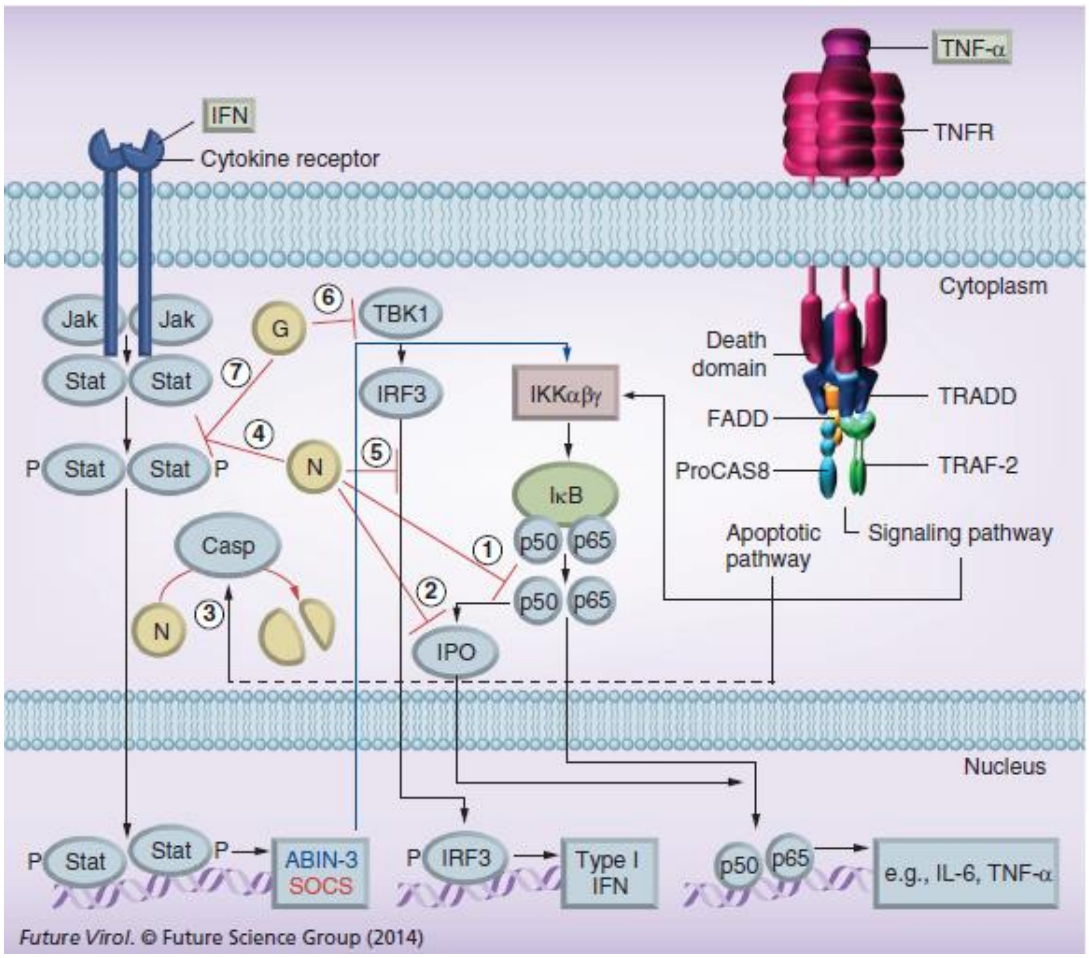

Figure 3. Molecular interactions of N protein. Shown in the figure is the suppression of the immune response during pathogenic hantaviruses infection and hantaviral proteins. The N protein inhibits NFκB's transport to the nucleus by binding importin-alpha proteins and NFκB complex (**1**); or importin-alpha proteins alone (**2**). The N protein can be cleaved by caspase 3 (**3**). The N protein is has been shown to be required for JAK/STAT signaling suppression and (4) type I IFN induction for some hantaviruses. The glycoprotein has also been shown to be involved in suppression of Type I IFN induction through TBK1 (**6)** and suppression of JAK/STAT signaling (**7**). Reproduced from Future Virology. (2014) 9(1), 87-99 with permission of Future Medicine Ltd.

Differences in which proteins are used by hantaviruses to inhibit amplification of IFN responses have been reported. Moreover, differences in induction of IFN-β RNA and protein have been shown following infection of human microvascular endothelial cells by ANDV (pathogenic) or PHV (nonpathogenic) [101]. ANDV suppressed IFN-β induction while PHV induced its activation; however, both viruses suppressed STAT1/2 phosphorylation and translocation [101]. Levine *et al.* showed that ANDV uses GPC and N protein to suppress IFN-β induction and IFN-dependent JAK/STAT signaling [75]. In that same report, SNV uses the GPC, but not N protein, to suppress IFN-β induction. In studies of the New York virus (NYV), a pathogenic, New World hantavirus closely related to SNV, the Gn-CT blocks RIG-I/TBK1 activation of IFN sequence regulatory element (ISRE) transcriptional responses, but the PUUV Gn-CT did not [66]. The NYV Gn-CT coprecipitates the N-terminal domain of TRAF3 [102]. The interaction of the NYV Gn-CT with TRAF3 is suggested to disrupt the formation of TRAF3–TBK1 complexes and inhibit induction of IFN-β [102]. Interestingly, the Gc-CT TULV, but not PHV, inhibit IFN-β and ISRE induction through TBK1, but not via TRAF3 [110]. Finally, the N protein of TULV has also been reported to be a weak antagonist of IFN-β induction [28]. Finally, HTNV has been shown to activate the Type III IFN, IFN-λ1, through a mechanism independent of Type I IFN [103].

In addition to suppression of IFN and JAK/STAT, the N protein down-regulates TNF-α receptor-mediated signaling by inhibiting activation of NFκB [104-107]. Studies in 293T cells suggest that the HTNV N, but not ANDV or

PUUV N, can block activation of NFκB by binding the importin-alpha proteins, which are responsible for NFκB's transport into the nucleus [107]. In a study by Ontiveros *et al.*, it was suggested that N may bind to both NFκB and importin as a complex to prevent its nuclear translocation [106]. Both studies also show that TNF-α induces degradation of IκB, implicating the block at NFκB's transport.

Inhibition of signaling pathways normally leading to activation of caspases and apoptosis is evident in cells expressing HTNV N protein [106] and ANDV N protein [86]. Furthermore, ANDV and HTNV-infected endothelial and epithelial cells are protected against staurosporine induced apoptosis [86, 106] and against cytotoxic granule-mediated induction of apoptosis [86]. Intriguingly, the suppression of caspase activity in HTNV N mapped to a highly nonconserved region from amino acids 270 to 330. In a study by Gupta *et al.*, it was shown that the ANDV N interacts with caspase 3 and granzyme B, resulting in inhibition of these apoptosis-inducing enzymes and cleavage of the N protein. Hence, hantavirus inhibits both granzyme B-mediated activation of caspase 3 and inhibits activated caspase 3 in infected endothelial cells targeted by natural killer (NK) cells, thereby protecting infected cells from being killed by cytotoxic lymphocytes [86]. In ANDV N, the caspase cleavage site mapped to DLID285, a site that is not conserved across New and Old World hantaviruses [86]. *In silico* prediction using GraBCas 1.0 [105] suggests potential caspase and granzyme B cleavage sites in N from other hantaviruses as well.

Conclusion

Diseases caused by hantaviruses cause a spectrum of vascular leakage in endothelial cells within the lung or kidney that can lead to shock and death. At present, there are no Food and Drug Administration (FDA) approved treatments and hence continued efforts on the mechanisms hantaviruses use to persist in their reservoirs and that cause disease in humans are essential to discovery of effective therapeutics. A number of recent studies show differences among the Old and New World hantaviruses in several aspects of their life cycle. Further, studies show there are striking differences in the immune responses following infection of hantaviruses within the reservoir and human. Despite the enormous progress that has been made in understanding the pathogenesis and immune responses of hantaviruses in humans and rodents, there is a large gap in molecular based knowledge of hantaviral proteins in their structures, functions and the mechanisms that facilitate the differences in the immune responses. Importantly, little is known about the specific viral determinants and viral protein-host interactions that drive these responses.

Significant gaps in knowledge remain in the entry, replication and assembly strategies used by hantaviruses. Further, structural studies have been challenging due to difficulty in purification of hantaviral proteins and the lack of a reverse genetics system, which have limited researchers ability to gain insight into function. Additionally, the majority of the studies that characterize the structure and function of hantaviral proteins have been conducted in Vero E6 cells or with viruses produced from Vero E6 cells.

In the past decade, *in vitro* primary endothelial and immune cells models have emerged to study the host responses elicited by hantaviruses in human and in a few cases rodent reservoirs. It is assumed that the structure and function of hantaviral proteins are the same within the Vero E6, human, and rodent reservoir, but further work to confirm similarities and differences remain. New insight into the virion structure suggests novel Class II mechanisms for binding to its receptor and assembly based on the tetrameric conformation. How the two hantaviruses with Cryo-EM structures interact with different receptors, β1 integrin for TULV, and β3 integrin for HTNV remains to be elucidated. In addition, distinct requirements for entry and trafficking of New and Old World hantaviruses suggest differences in these mechanisms. Whether these differences also extend to rodent reservoir endothelial cells is not known. Finally, recent findings suggest that hantaviruses regulate TNF-α and INF-induced responses as well as apoptosis within infected endothelial cells and nearby immune cells. These studies also underscore differences in strategies among the hantaviruses in the use of the N, NSs and/or G_N tails in modulating host response. While some N protein – host protein interactions have been uncovered, additional studies are needed to define the precise mechanisms across hantaviruses. Finally, studies show the potential importance of the CTL responses in causing disease and also in protection depending on the virus. Clear answers await further analysis of the CTL-response in many more patients across the major hantaviral diseases.

Future perspective for treatment

Design and development of vaccines and antivirals for treatment of hantaviral infections remains challenging. Continued advancement of vaccines and antivirals would be greatly accelerated with knowledge gained from future research focused on the structure and function of hantaviral proteins during entry, fusion, replication and assembly. For example, knowledge of the glycoprotein spike structure will enable insight into neutralization epitopes that can be incorporated into vaccination technology. Knowledge of viral sites of replication and assembly of HTNV within cells will benefit discovery of new targets for antiviral drug discovery. Furthermore, future efforts that define the cellular components that interact with viral proteins may reveal potential therapeutic targets. Using current and newer approaches in structural and molecular virology, one can begin to unravel sites and mechanisms of binding, replication and assembly of hantaviruses within cells. These types of studies will be important in revealing unique aspects of the viral life cycle that have presumably thwarted the field's ability to generate recombinant viruses to study the function of viral proteins.

In addition to understanding the structure and function of hantaviral proteins, it is clear that unraveling the differences in immune responses in their reservoirs and humans may shed important light into novel approaches for treatment of these serious diseases [100]. Breakthroughs in the study of immune responses of hantaviruses in rodent models will require the active development of new reagents in lethal models of disease (e.g., hamster) and persistence (e.g.,

deer mouse). The recent sequencing of hamster and deer mouse genomes is an important new development in that regard.

CHAPTER II

THE MURINE MODEL FOR HANTAAN VIRUS-INDUCED LETHAL DISEASE SHOWS TWO DISTINCT PATHS IN VIRAL EVOLUTIONARY TRAJECTORY WITH OR WITHOUT RIBAVIRIN TREATMENT

Introduction

We are interested in how hantaviruses adapt, and hence evolve, in a nonreservoir rodent host. In nature, hantaviruses have high selectivity of infection for a single reservoir host species. However, phylogenetic analyses clearly show that spillover and adaptation of hantaviruses to nonreservoir hosts has occurred throughout the evolutionary history of *Hantavirus*. Recent evidence suggests these spillover events have occurred not only across different genera, but also between different orders of mammals [108-111]. Understanding spillover and the emergence of new pathogens in new hosts is critical for safeguarding global health, both wildlife and human. Spillover of pathogens is the first step leading to the emergence of new strains, new emerging diseases and potentially, pandemics. Alarmingly, the “spillover” and subsequent adaptation of viruses to new hosts in nature is an area of biology of which we have little understanding. In this chapter of my thesis, I evaluated the Hantaan virus in *Mus musculus* over time following infection. The goal was to determine if any changes occurred in the viral genome over time in the presence and absence of ribavirin. We have

previously shown that ribavirin increases the mutation rate of Hantaan virus in vitro. We hypothesized that ribavirin would increase the error rate in vitro and drive the virus to lethal extinction as observed in vitro [112]. While we did observe the expected increase in the mutation frequency of the viral genome to what we observed in vitro, ribavirin appeared to increase the ability of Hantaan virus to persist. My contribution to the publication was in the analyses of the viral sequences sampled over time. In the following I give further background than provided in the manuscript on the evolution and some of the tools one can use to evaluate evolutionary changes.

Mechanisms of viral evolution

The three major mechanisms of viral evolution include Antigenic Drift (AGD), Antigenic Shift (AGS) and recombination [8, 113-116]. Each of these processes have the potential to result in a genetic change in a coding region that may alter protein function and therefore phenotype. AGD is an intrinsic process where a gene drifts due to misincorporation of nucleotides/nucleosides in genes during synthesis of the genome or copy of the genome by the viral polymerase. This natural rate of mutation has the possibility of producing both silent and missense mutations. A missense mutation or nonsynonymous mutation can arise due to the misincorporation of a single nucleotide which results in a codon for a different amino acid. In RNA viruses the process of misincorporation has enormous impact on viral evolution, because the viral polymerase (RdRp) has a high error rate or lower fidelity than found in the vast majority of host cellular

polymerases. Generally, as the RdRp synthesizes new RNA genomes, the wrong nucleotide is misincorporated can range from 10^3-10^4. For hantavirus with a genome of approximately 12,000 nucleosides this may results in 1 nucleotide change per genome per round of replication [8].

AGS is the process in which two viral strains exchange parts or entire viral gene segments. This is common in segmented viral RNA genomes such as hantaviruses and influenza viruses. AGS occurs when two virus strains infect the same host cell and genomes are packaged with a reassortment from the two viruses. Reassortment has been shown to occur with hantaviruses in natural wildlife settings [117].

Recombination is similar to AGS except it is the reorganization/orientation of alleles in a single gene segment which results in a new phenotype. In Europe a phylogenetic examination of TULV N protein harbored by *Microtus arvalis* found in Slovakia revealed two lineages from different regions that arose through recombination [114].

The three aforementioned mechanisms of viral evolution can be influenced by intrinsic (within-host) and extrinsic (between-host and environmental) factors. Each of these factors can play an important role on the success or failure of transmission to new hosts and the replication or life cycle within-host. Both intrinsic and/or extrinsic pressures within a host can promote and drive the selection of genetic alterations, directly or indirectly. Examples of extrinsic pressures that can affect transmission rates of viruses among rodent hosts are any changes in food, predators and water. In the instance of increased

predators or decreased food there would be changes in biodiversity and population structures of rodents in that community. In turn this would influence the number of infections of a single host over time. If the basic reproductive value (R_0) falls below the rate required for maintenance of the virus in nature, the infection will die out in that population. Alternatively, an increase in the number of susceptible individuals in the community could drive spread and prevalence. This extrinsic pressure could be supplied by an increase in food, which can increase the number of litters per year and hence the rodent population. Population increases can also result in increased interaction among rodents through breeding and fighting and thus an increase likelihood of a virus transmission to occur, in particular, to nonreservoir rodents.

A Genetic Selective Sweep (GSS) occurs when a mutation results in an amino acid change in the genome that gives rise to a viral phenotype that is more fit to survive than its peers. A site under diversifying selection may confer a phenotype to the population that has increased fitness. The newly emerged viral genotype may not be dominant, however, and until it reaches greater proportions in the population, the new genotype may not confer its advantage to the overall population [118]. This is due to the lag time it takes for the newly produced virus (now under purifying selection) to become the prominent phenotype in the population. GSS are most of the time due to bottle neck events (due to extrinsic or intrinsic pressures). The emergence of positively-selected amino acids or nonsynonymous amino acids can be identified using various bionformatic approaches and will be reviewed in the following.

Tools for evaluation of genetic changes in viral genomes

Nonsynonymous amino acid changes are known as positively selected amino acids. Positively selected amino acids are identified on a site by site (by codon) basis. A common approach is to search amino acids within a coding region for nonsynonymous error rate *(dN*) greater than the synonymous error rate (*dS*). If the nonsynonymous error rate (*dN*) is greater that a synonymous error rate (*dS*), or a (*dN*/*dS*)>1.0, this suggests positive selection has occurred. In order to determine what sites are under positive selection the web server "DataMonkey" can be used to conduct the analysis (http://www.datamonkey.org), using alignments of the coding regions within a RNA population.

Since 2010 DataMonkey has been used by the scientific community in over 100,000 analyses for amino acids under selection [119, 120]. The analyses that DataMonkey conducts are Single Likelihood Ancestor Counting (SLAC), Mixed Effects Models of Evolution (MEME), Fixed Effects Likelihood (Fel), internal Fixed Effects Likelihood (iFel), & Fast Unbiased Bayesien AppRoximation (FUBAR) (**Table 1**) [119, 120]. The SLAC, Fel, and iFel analysis are directed to finding amino acid sites that may have been affected by purifying or diversifying selection across multiple sequences in an alignment [119, 120]. iFel is slightly different than Fel in that is restricted to finding amino acid sites under positive selection in sequences that are within the internal branches of the Phylogenetic Tree (created by DataMonkey)[119, 120]. MEME is like Fel and iFel except that it has a less conservative test statistic (ω) which leads to less Type I error (the incorrect rejection of the null hypothesis) [119, 120]. The FUBAR

analysis is like MEME in that it has more computing power than SLAC, Fel, and iFel [119, 120]. FUBAR although can be used to determine positively selected amino acids in large datasets [119, 120]. When all analysis are conducted together on the same dataset it is certain that all amino acids under positive selection are identified and recombination is taken into account [121].

Herein, we have used these approaches to examine the evolution of Hantaan virus in a mouse model of lethal infection in the presence and absence of ribavirin. There are two intrinsic pressures afforded by this model. First, infection of HNTV in this host represents a spillover infection of a nonreservoir rodent host. The virus is not adapted to this host and hence to survive or persist as it does in wild mice in nature. Hence, the virus must undergo genetic changes that would be favorable for survival. Secondly, we used ribavirin. We have shown that ribavirin increase the mutation frequency of the RdRp *in vitro*. Hence, ribavirin alters the intrinsic environment of the virus-host interaction.

Table 1.

Datamonkey analysis for determining selection

Method	Description
Single Likelihood Ancestor Counting (SLAC)	Identifies Sites in a multiple sequences alignment that have been affected by positive of negative selection using likelihood branch lengths, nucleotide, and codon substitution parameters (*dN*) and (*dS*).
Mixed Effects Models of Evolution (MEME)	Identifies positive, negative and episodic selection (large proportion of positively selected sites; multiple positively selected sites within one sequence) at the level of individual nucleotide sites.
Fixed Effects Likelihood (FEL)	A codon based maximum likelihood test that identifies sites in a multiple sequences alignment that have been affected by positive of negative selection. The parameters (*dN*) and (*dS*) for this test are determined independently for each codon site.
internal Fixed Effects Likelihood (iFel)	A codon based maximum likelihood test that identifies sites under positive and negative selection that are restricted in sequences in the interior branches of the tree.
Fast Unbiased Bayesien AppRoximation (FUBAR)	Newest codon based maximum likelihood test that vastly improves speed of analysis. Parameters for this test are determined independently for each codon site and across codon sites.

In vivo model of hantaviral infection

Laboratory animal models of hantaviruses have proven useful for basic research to study infection and virulence [122-125] and for the discovery of therapeutics and potential vaccine candidates [126-131]. For example, the well-established lethal, suckling mouse model of HTNV infection demonstrated ribavirin's therapeutic efficacy [129] and provided the impetus for clinical studies of its efficacy in humans [128, 130]. Ribavirin was recently shown to have efficacy *in vivo* in the lethal hamster model of ANDV, a New World hantavirus [131]. Clinical studies of intravenous ribavirin treatment of HFRS in human cases caused by HTNV have shown efficacy, with a decrease in occurrence of oliguria (decreased urine output) and severity of renal insufficiency [130]. No other treatment is available for either disease.

The study of an antiviral both *in vitro* and in an animal model of disease progression is important for a complete understanding of its mechanism of action and potential for selecting for drug resistance or lethal mutagenesis [132-135]. Lethal mutagenesis is a chemotherapeutic strategy in which one uses a viral mutagen to promote the lethal accumulation of mutations in an RNA viral genome. Ribavirin is a potent, broad-spectrum antiviral for many RNA and DNA viruses *in vitro* and *in vivo* [136]. The antiviral activity against several viruses is due to its ability to competitively inhibit inosine monophosphate dehydrogenase (IMPDH) [137, 138], a key enzyme in the *de novo* synthesis of GTP. Additional targets for its antiviral activity have been shown, including capping [139], translation efficiency of viral mRNA [140], and a direct suppressive effect on the

viral polymerase activity [141-143]. Ribavirin can also act as a potent RNA virus mutagen for several RNA viruses and can cause error-prone replication [135, 144-147]. In addition to targeting the purine metabolic pathway and viral enzymes, recent studies suggest that ribavirin may act by promoting a type 1 immune response [148]. Specifically, Kobayashi et al. showed that ribavirin can down modulate interleukin-10 (IL-10)-producing Treg 1 cells, which could inhibit the conversion of $CD4^+$ $CD25^-$ $FOXP3^-$ naive T cells into $CD4^+$ $CD25^+$ $FOXP3^+$adaptive Treg cells to maintain Th1 cell activity [149]. The role of the ribavirin-induced immune response in acting as a selective pressure on hantaviral population and evolution has not yet been addressed.

In vitro, we have shown direct effects of ribavirin on HTNV through the host IMPDH and viral replication [150], which correlates with an increase in mutations in the vRNA genome [151, 152]. Our studies on the mechanism of action of ribavirin's potent antiviral activity have also provided insight into the standing genetic variation and population structure of HTNV [151, 152]. These studies revealed an increase in the mutation frequency in the viral population, after which the mutation frequency did not correlate with a dose-dependent decrease in the level of viral RNA, Plaque Forming Units (PFU), or [RTP]/[GTP]. Intriguingly, even at the highest concentrations of ribavirin-treated cells, the proportion of HTNV wild-type sequences never dropped below 60% for the target S-segment sequence used in sampling. These studies suggested that HTNV could not survive past a critical mutational burden or lethal threshold.

Based on the findings of our prior studies [151, 152], we sought to test whether mice infected with HTNV and treated with ribavirin would show an increase in mutation frequency and demonstrate a lethal extinction threshold. Specifically, would ribavirin cause extinction as revealed by an increase in viral mutation rate followed by a steady decrease in titer *in vivo*? We found that, surprisingly, untreated, HTNV-infected mice showed an overall apparent decrease in mutational frequency compared to the previous mutational frequencies measured for the HTNV seed stock in Vero E6 cells [151, 152]. In contrast, ribavirin-treated, HTNV-infected mice showed an increased mutational load. Both populations showed a reduction in specific infectivity over time. These studies show, for the first time, two distinct evolutionary trajectories for HTNV within a lethal mouse model of disease in the presence and absence of ribavirin, as well as evidence for positive selection not previously observed *in vitro*. In the ribavirin-treated vRNA population, analyses of rates of nonsynonymous (*dN*) and synonymous (*dS*) substitutions in the S segment revealed a positive selection for codons within the HTNV N protein gene, while untreated, HTNV-infected mice showed purifying selection. Furthermore, in contrast to our prior *in vitro* studies [151, 152], the increased mutational load did not lead to lethal extinction. Intriguingly, viral RNA levels remained high in both untreated and treated populations, with a decrease in the level of infectious virus over time. The levels of infectious virus produced by the two populations, however, were statistically significantly different, reflecting a difference in the selective pressure by the host with and without ribavirin. Importantly, these data reveal that while the virus

populations within the ribavirin-treated, HTNV-infected mice had a larger proportion of deleterious mutations leading to a smaller number of infectious particles, they harnessed the increased mutation rate to also achieve genetic changes that improved their survival over that of the wild type. Finally, while a direct analysis of the potential for ribavirin-induced immune responses as an added selective pressure was not possible in the context of this experiment, the immune system of the suckling mouse model was assessed at the time point for ribavirin treatment, which was 11 days postnatal (dpn) or 10 dpi. These studies showed a responsive innate immune system in these young mice.

Materials and Methods

Cells and viruses

Vero E6 cells (CRL-1586; ATCC) were propagated and used for production of HTNV strain 76-118 and measurement of virus in tissue samples. Cells were cultured in Dulbecco's modified Eagle's medium (DMEM; Invitrogen) supplemented with 10% fetal bovine serum (FBS), 1% penicillin-streptomycin, and 1% L-glutamine (Sigma). The titers of virus in the seed stock and in animal tissues were measured by determining the numbers of PFU per ml, using an agarose overlay method as described previously[153].

Animal study

ICR suckling mice (Harlan, Prattville, AL) were used for all animal studies and were individually identified by tattoo. Pregnant mice were housed singly with

their pups in solid-bottom polycarbonate cages on stainless steel racks in an environmentally monitored, well-ventilated room. Bedding (P. J. Murphy Forest Products, Inc., Montville, NJ) was used in the bottom of the cages. Dams were fed on certified rodent diet 5002 (PMI Feeds, Inc., St. Louis, MO), and tap water was provided *ad libitum* during the study periods. Procedures used in this study were designed to conform to accepted practices and to minimize or avoid causing pain, distress, or discomfort in the animals and were approved by the Institutional Animal Care and Use Committee (IACUC) at Southern Research Institute.

Animals were monitored for a 26-day period following intracranial (i.c.) challenge with HTNV (strain 76-118). On day 0, each mouse in group 1 received 10 µL DMEM and each mouse in groups 2 and 3 received 10 µL of 1×10^3 PFU HTNV diluted in DMEM. Beginning at 11 dpn or 10 dpi, each mouse was treated with ribavirin (MP Biomedical, Inc.) via the intraperitoneal (i.p.) route at 5 µL/g of body weight (50 mg/kg of body weight) for 15 days. All mice were observed twice daily throughout the study periods for signs of morbidity and mortality and for body weight, and detailed observations were recorded daily beginning at −1 dpi.

Isolation of total RNA, cDNA synthesis, and real-time RT-PCR

Briefly, total RNAs from infected tissues were homogenized and extracted with TRIzol (Invitrogen), and 0.5 µg of total RNA was subjected to a reverse transcription (RT) reaction with SuperScript III reverse transcriptase (Invitrogen). The HTNV S-segment vRNA copy number within virus-infected mouse tissues

was measured with a real-time RT-PCR assay using the comparative threshold cycle method, i.e., $2^{-\Delta\Delta}CT$ method [150, 151]. Real-time PCRs were performed in triplicate for each sample and were prepared with TaqMan universal PCR master mix (Applied Biosystems).

Sequencing and phylogenetic analyses

cDNAs were cloned and analyzed for each lung tissue as described previously [151]. Briefly, cDNA prepared as described above was amplified by a PCR using Phusion High-Fidelity DNA polymerase (Finnzymes Oy, Finland) following the manufacturer's protocols. Primers HS24 (forward primer; 5′-TACTAGAACAACGATGGCAACTATG-3′) and HS1336 (reverse primer; 5′-GTGCAAATATGATTGATAATGATTCAGTAG-3′) were used to amplify the open reading frame of N within the S-segment gene. The amplified product was cloned into the pCR-4 plasmid (Topo cloning kits for sequencing; Invitrogen) after A tailing by using *Taq* polymerase (Promega). On average, 96 colonies per lung were subjected to colony PCR using the M13 forward and M13 reverse primers [151]. As a control, the background mutation frequency (inherent in the amplification process) was measured using the same enzymes and plasmid DNA encoding the HTNV S-segment cDNA.

SeqScape 2.1 was used to generate the open reading frame (from codons 19 to 430) of the plus strand of the HTNV S-segment forward and reverse sequences from each of the clones from each lung. The ABI file of each sequence was evaluated manually, and sequences with inconclusive nucleotides

(nt) at any position, stop codons, or gaps were removed. Sequences were exported into fasta file format, aligned by ClustalW in Mega 5.1 [154], and compared to the published HTNV 76-118 sequence (GenBank accession number M14626) as well as other sequences to generate phylogenetic trees [155]. Mutation frequencies for each sample were calculated from the alignment of individual cDNA sequences with that of HTNV 76-118. Phylogenetic analyses based on maximum likelihood or neighbor-joining programs were generated from the ClustalW alignments in Mega 5.1, with 1,000 bootstraps [154].

Ratio of nonsynonymous to synonymous substitution rates

The ClustalW alignments for the mock-treated and ribavirin-treated groups defined above were analyzed by the Web server Datamonkey [119]. The sequence sets were analyzed by single-likelihood ancestor counting (SLAC), fixed-effects likelihood (FEL), internal fixed-effects likelihood (IFEL), mixed-effects model of evolution (MEME), and fast unbiased Bayesian approximation (FUBAR), using default settings) [119]. Datamonkey removed all identical sequences, which left 32 and 107 sequences that differed in the mock-treated and ribavirin-treated groups, respectively. Automatic model selection identified the HKY85 nucleotide substitution bias model.

Statistical analyses

Statistical analyses of virus loads from the animal study were performed using R, a language and environment for statistical computing and graphics

(www.r-project.org/). A set of generalized linear models (GLM) were used to test the main effects of treatment (mock or ribavirin) and dpi on viral load (given by vRNA copy number, number of PFU, or number of PFU/vRNA copy) in mice. Full models including an interaction term were included in the goodness-of-fit assessments, and all simpler models were considered to define the accepted model used in interpretation of data. Only data from time points after the ribavirin course of treatment were included in the analysis (i.e., ≥12 dpi). Day 26 was not included in the analyses. Best-fit statistical models were selected using log-likelihood ratio estimates and the Akaike information criterion (AIC). In cases where single effects models were the best fit to explain the data, nonparametric statistical tests were used to describe the difference between groups. In all analyses, the type I error rate was set to an α level of 0.05.

Results

Study design

To define the intrahost mutation frequency and population structure of HTNV following infection in mock- and ribavirin-treated, HTNV-infected mice, we employed a standard experimental design and lethal murine model of HTNV that is used to measure antiviral efficacy (**Table 2**) (**12**). One-day-old suckling mice were infected with 1,000 PFU of HTNV, and from 10 to 24 dpi, mice were treated once per day with 50 mg/kg of ribavirin. Mice were sacrificed as noted in **Table 2**, and lung tissues were harvested and flash frozen in liquid nitrogen. At the same time that this study was conducted, an efficacy study of an analog of ribavirin

was conducted in parallel [156]. The mean time to death (MTD) and percent survival in ribavirin-treated, HTNV-infected mice published as part of that study were 18.5 days and 35%, compared to 15.5 days and 10% survival for untreated, HTNV-infected mice [156]. In the groups presented in **Table 2**, the mock-treated, HTNV-infected mice that survived to day 26 were moribund, and the virus was below the limit of detection by plaque assay. The day 26 time point was not included in our analyses.

Table 2.

Group, treatment and sampling design

Group/ Treatment	DPN*	5	9	11	13	15	18	18	21	22	27	Total (mice)
	DPI**	4	8	10	12	14	17	18	20	23	26	
Group 1: No Virus (mock)				2		2		2				6
Group 2: HTNV		2	2	2	3	5*	2	2	0	1	3	16
Group 3: HTNV & RBV		0	0		3	3	1		3	0	3	14

*DPN- days post-natal, **DPI-days post-infection

Viral titers in lungs in mock- and ribavirin-treated mice

Lung tissue was harvested and analyzed for S-segment vRNA copy number by real-time RT-PCR and for number of PFU for both mock- and ribavirin-treated, HTNV-infected mice (**Figure 4**). In the mock-treated group, the vRNA copy number increased through day 12 and remained fairly constant in the few mice that survived from days 14 to 24 (**Figure 4A**). Similarly, in the ribavirin-treated group, the vRNA copy number remained steady from days 14 to 26. GLM testing and statistical comparison of vRNA levels (days 12 to 20) in the mock-treated and ribavirin-treated groups showed that they differed significantly (Wilcoxon rank sum test; $P = 0.035$). These data showed that the ribavirin-treated group had more vRNA copies on days 12 to 20 than the mock-treated, HTNV-infected mice.

In the mock-treated, HTNV-infected mice, viral titers measured by plaque assay increased through day 9 (**Figure 4B**). After day 9, mock- and ribavirin-treated, HTNV-infected mice showed similar levels of PFU over time. GLM model fitting confirmed that the dpi-only model was the best fit to explain the variance in numbers of PFU, and analysis of variance (ANOVA) showed no significant effect of treatment (with or without ribavirin) on the number of PFU, controlling for dpi ($P = 0.84$).

We calculated and plotted the selective infectivity (number of PFU/vRNA copy) over time (**Figure 4C**), as we have found this valuable for comparisons made across groups and experiments conducted *in vitro* [151]. Analysis of the data by GLM showed that treatment only was the best model to explain the

variation in the data. Therefore, we used a nonparametric Wilcoxon rank sum test to compare these two groups, ignoring changes over time, to determine if there was a difference in the PFU/vRNA ratio due to ribavirin treatment. These data suggest that the specific infectivity for the ribavirin-treated, HTNV-infected mice was lower than that for untreated mice ($P = 0.053$). A model of the probability density for each population is shown in **Figure 4D**.

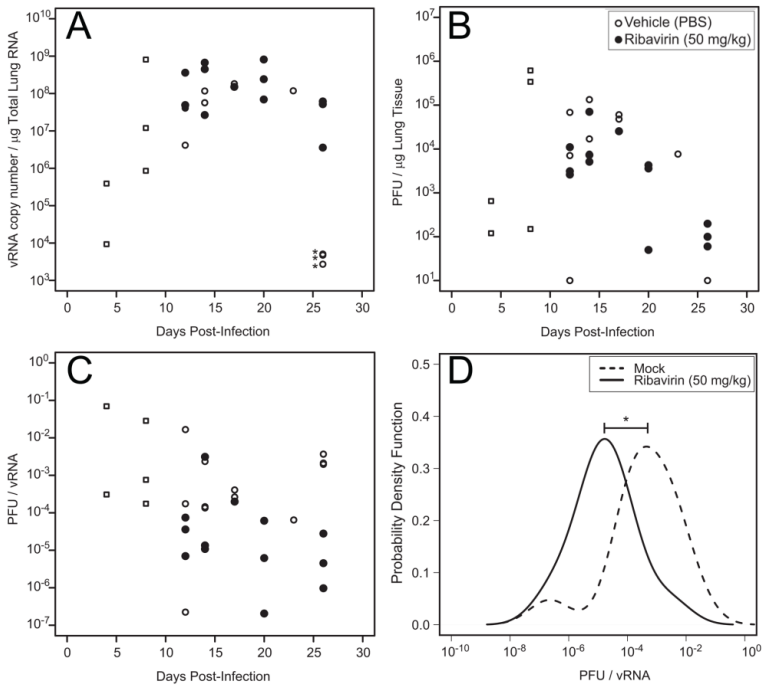

Figure 4. Viral RNA and infectious virus levels in lung tissue of untreated and ribavirin-treated, HTNV-infected mice. (**A**) Lung tissue was homogenized from each animal specimen and divided to measure the copy number HTNV S-segment vRNA per gram (g) of tissue in mock-treated (open circles) and ribavirin-treated (solid circles), HTNV -infected mice and (**B**) the levels of infectious virus in lung tissue suspension by PFU. Asterisks indicate vRNA-positive samples from animals that were moribund, infectious virus from these animals were below the limit of detection inplaque assays and were eliminated from the subsequent analyses of selective infectivity. Open squares indicate untreated, HTNV-infected, but are noted differently since statistical comparisons did not take these time points into consideration. In (**C**), the selective infectivity (PFU per vRNA copy number based on gram of lung tissue) is plotted by days post-infection for HTNV-infected mice that were treated with DPBS or ribavirin from 10 to 25 dpi. In (**D**), smoothed histograms (probability density functions) of

the selective infectivity for each group, HTNV-infected mice (dashed line) and HTNV-infected, ribavirin-treated mice (solid line). The Wilcoxon Rank Sum show that there was a significant reduction in PFU/vRNA in ribavirin-treated mice, including only samples from 12-25 dpi ($p = 0.053$).

Intrahost genetic variation of HTNV in untreated and ribavirin-treated mice

Using a previously standardized approach to measure the mutation frequency of HTNV [151], estimates of nucleotide and amino acid (aa) mutation frequencies were made for each viral population in each mouse lung (**Table 3**). Briefly, total RNA was isolated, and S-segment cDNAs were PCR amplified, cloned, sequenced, and aligned using ClustalW. The region cloned was the open reading frame of the N protein. Changes from the master consensus (HTNV seed stock) were counted, and the estimated mutation frequency per 10,000 nucleotides or 3,333 amino acids is shown (**Table 3**). Our prior analyses for standardization of the method showed that an accurate assessment of mutation frequency is reached with a sample size of 48 clones for each sample, after which no change in the proportion of genetic variation or frequency is noted[151]. The number of cDNAs examined for each mouse lung sample is shown in **Table 3**, after removal of sequences with stop codons, gaps, or poor sequence information. For this analysis, we used a total of 653 sequences for the ribavirin-treated, HTNV-infected group, among which 107 sequences showed nt/aa differences from the consensus sequence. For the mock-treated, HTNV-infected group, we used a total of 408 sequences, among which 32 showed nt/aa differences.

On day 8 post-infection, the estimated standing genetic variation in the mock-treated animals ranged from 0.51 to 0.84 mutation per 10,000 nt (**Table 3**; **Figure 5**). Our previous *in vitro* estimates show that HTNV has an estimated average mutation frequency of 1.1 to 1.4 mutations per 10,000 nt in Vero E6 cells

[151]. In the mock-treated mice, the mutation frequencies of the HTNV population showed a nearly 2-fold decrease (**Figure 5**) ($P < 0.05$). On average, 0.5 mutations per 10,000 nt was estimated overall from days 8 to 23. In contrast, in HTNV-infected mice treated with ribavirin, the average mutation frequencies from days 12 to 20 (2.3/10,000 nt) or days 12 to 26 (1.8/10,000 nt) were 3- to 4-fold higher ($P < 0.05$) (**Table 3**; **Figure 5**).

We further examined the mutational frequency of HTNV in mock-treated and ribavirin-treated mice by the specific infectivity, i.e., the number of PFU/vRNA copy (**Figure 6**). The hatched line in **Figure 6A** shows the mutation frequency of approximately 1.1 mutations per 10,000 nt measured *in vitro*. The graph shows a flattening of specific infectivity with increased genetic variation in the population (ribavirin-treated mice). For the mock-treated group, the specific infectivity falls below this mutation frequency, while more than half of the ribavirin points fall above this line (**Figure 6A**). Analysis of these data by a probability density function showed that the mock-treated, HTNV-infected mice had a sharp narrow peak with decreased mutations, while the ribavirin-treated group had a broader and lower peak of distribution (**Figure 6B**). Levene's test for equal variance showed that HTNV-infected, mock-treated mice had marginally significantly more variance than ribavirin-treated animals ($P = 0.067$) (**Figure 6B**).

Table3.

Summary of mock & ribavirin-treated mutation frequencies

Mouse ID	Day	No. Nt. Changes[1]	Total No. cDNAs		Nt. Mutation Frequency ($x10^{-5}$)	AA Mutation Frequency ($x10^{-5}$)
Mock-treated, HTNV-infected						
1007	D8	5	48		8.4	20.2
1009	D8	2	32		5.1	7.6
402	D12	4	44		7.4	16.6
404	D12	2	45		3.6	16.2
504	D12	4	48		6.7	15.2
308	D14	0	31		0	0
303	D14	4	37		8.8	6.6
407	D17	1	43		1.9	5.6
305	D17	2	33		4.9	0
401	D23	1	47		1.7	0
TOTAL		**25**	**408**	**AVE**	**5.4**	**12.6**
Ribavirin-treated, HTNV-infected						
1012	D12	11	43		20.7	33.9
1013	D12	2	44		3.7	11.0
1201	D12	4	42		7.71	23.1
1105	D14	12	117		8.3	12.4
1112	D14	4	40		8.1	18.2
1204	D14	16	45		28.8	37.8
1102	D17	2	35		4.6	13.9
1209	D20	10	43		18.8	45.1
1208	D20	4	15		21.6	64.7
1207	D20	5	47		8.6	20.7
1109	D26	23	42		44.3	98.2
1101	D26	15	95		12.8	28.1
1110	D26	27	45		48.5	97.1
TOTAL		**135**	**92**	**AVE**	**18.2**	**38.9**

[1]based on a 1236 nucleotide (nt) of cDNA; [2]total number of cDNAs analyzed per mouse

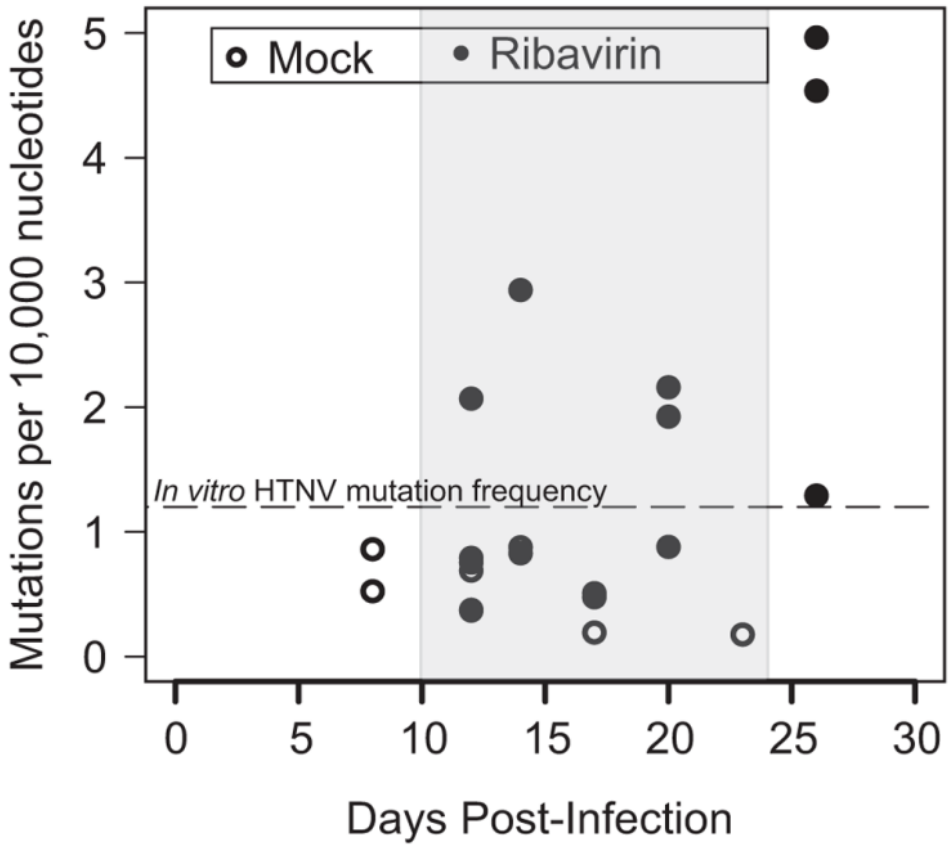

Figure 5. Average intrahost genetic variability of HTNV population in mock- and ribavirin-treated mice. Mice were infected with 1000 pfu of HTNV by intracranial injection on day 1. After ten days, mock vehicle or ribavirin 50 mg/kg was administrated once per day for 14 days.

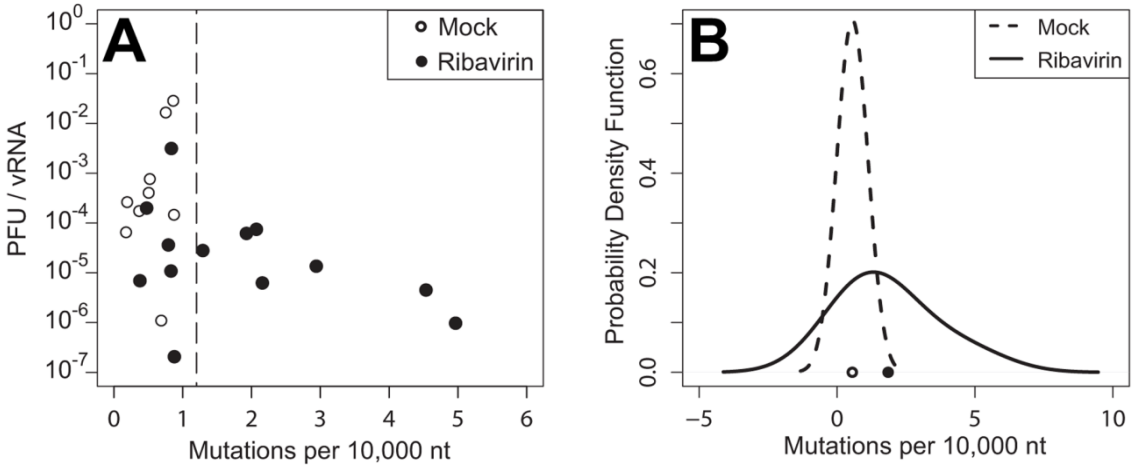

Figure 6. Selective infectivity of animals from untreated and ribavirin-treated animals. (**A**) The mutation frequencies for individual animals from mock- and ribavirin-treated infected groups were plotted against their selective infectivity (PFU/vRNA copy number). The hatched area represents the range of the starting HTNV seed stock material measured in Vero E6 cells *in vitro*. (**B**) Smoothed histograms (probability density functions) of vRNA mutation frequency (mutations per 10,000 nt) in tissues of mock- and ribavirin-treated HTNV infected mice show that RBV-treated animals have higher variance in mutation rate (Levene's test, $p = 0.067$). Smoothing bandwidth for mock- and ribavirin-treated groups are 0.5 and 1.5, respectively.

In **Table 4**, the amino acid changes from the consensus (HTNV 76-118) are presented for each mouse in each of the treatment groups by day. A larger number of amino acid changes (92 in total) was noted in the ribavirin-treated, HTNV-infected group than in the mock-treated group (16 in total). Of those amino acids with a change, 29/92 amino acids showed a gain or loss of negative/positive charge (**Table 4**). The distribution of amino acid changes along the protein shows some clustering (**Figure 7**). The mock-treated group showed 13 of 16 changes in the first half of the N protein. The distribution of amino acid changes predominated throughout the N protein in the ribavirin-treated group. Interestingly, a greater percentage (42%) of those changed in the amino and carboxyl termini (first and last 110 aa) had changes in charge. In contrast, the central region had many fewer (20 to 30%) changes in charge.

Table 4.

Amino acid changes within HNTV S-segment in mice

DPI	Mouse ID	Amino Acid Changes* Mock-Treated	Mouse ID	Amino Acid Changes* Ribavirin-treated
8	1007	E33G, R268Q, I325Fx2	-	-
8	1009	P182S	-	-
12	402	none	1012	R26G, D37G, D59G, G99C, R156W, A410E
12	404	V19E, D80Y, R282K	1013	Q55R, V84A
12	504	G63R, Q79H, G196D	1201	Y265N, A291V, T318I, N423S
14	308	n.d.	1105	A28T, K77R, M140I, K211E, E277G, L320M
14	303	D110G	1112	K30R, P174S, H176Y
14	-	-	1204	M95I, L120R, F165R, R267Q, S333F, A410G, D415N
17	407	I122T	1102	A208V, D394N
17	305	none	-	-
20	-	-	1209	G72R, M95I, D118N, A212V, L255F, A330V
20	-	-	1208	K41M, P132L, G204R, R263K
20	-	-	1207	A70T, K245R, E280D, R367K
23	401	none	-	-
26	-	-	1101	(A70V,G87E),D59N, E192K, R197K, A229V, E237G, P243S, I305T, A344V, D394N
26	-	-	1110	(R68K,P81L, L246F),(D88N,G99S, A288V), M188I, D167N, V130I, P182L, A227V, I193V, A260T, A260V, M295I, G310E, T318I, A387T
26	-	-	1109	S121N, T142I, R144K, S164L, Q196H, R199Kx3, C203Y, P218S, V222L, P248S, A251T, G257D, T278I, K358E, E425K

*changes from wildtype HTNV 76-119 consensus sequence

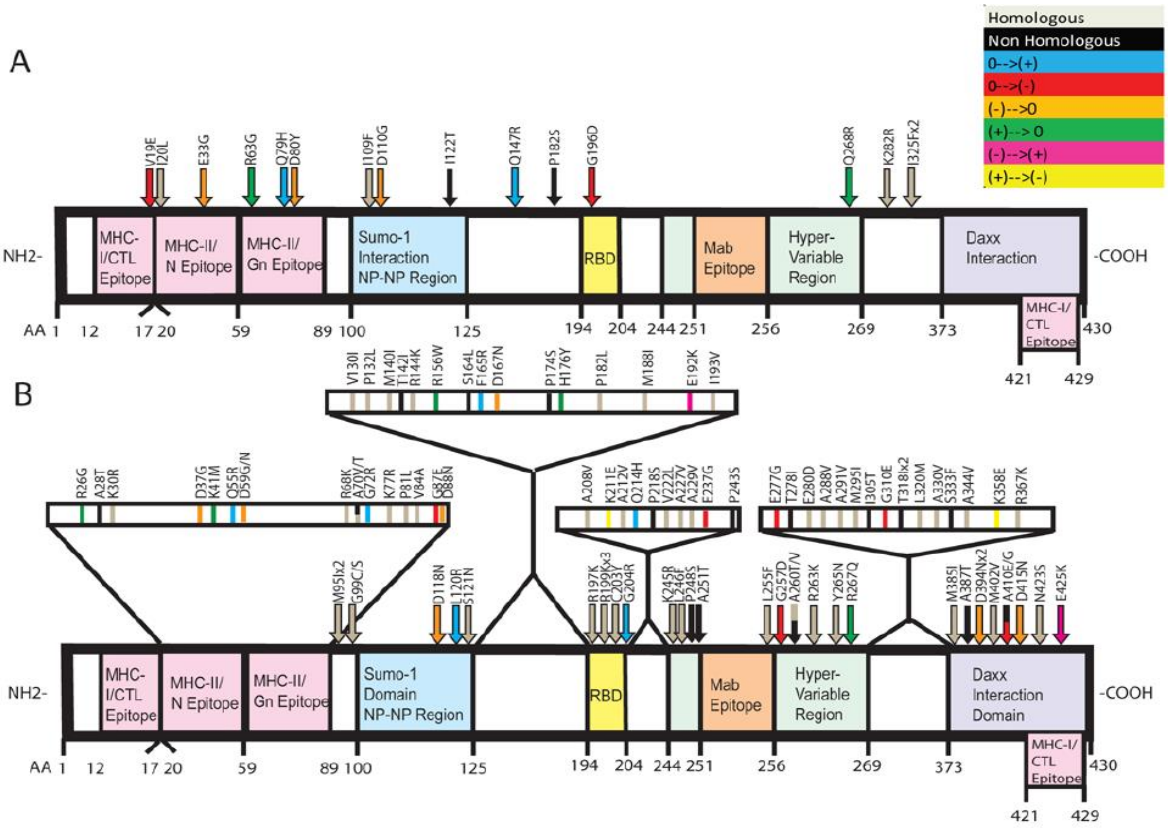

Figure 7. Illustration summarizing the locations of amino acid changes in the HTNV N protein. The amino acid changes from the HTNV wild-type N protein sequence identified in mock-treated (**A**) and ribavirin-treated (**B**), HTNV-infected mice are noted at the top. Corresponding colors reflect changes in amino acid charge. Functional domains within the N protein that have been identified in the literature are noted.

Phylogenetic relationships of sequences

Nucleotide and amino acid alignments were made with 654 sequences from the ribavirin treatment group and 418 sequences from the mock treatment group. The consensus sequences from other strains and species of hantaviruses reported in GenBank were included in the alignment (GenBank numbers are available upon request). From the alignments, 546 of the 654 ribavirin treatment group sequences and 386 of the 418 sequences from the mock-treated group were identical. The best-scoring maximum likelihood trees for mock-treated (**Figure 8A**) and ribavirin-treated (**Figure 8B**) mice, with additional wild-type sequences from Hantaan viral strains, are presented. As predicted from the mutation frequencies, the number of sequences showing nucleotide differences (light blue) and bifurcation was greater in the ribavirin-treated group (**Figure 8B**) than in the mock-treated group (**Figure 8A**). Tests for positive selection are discussed in the following section.

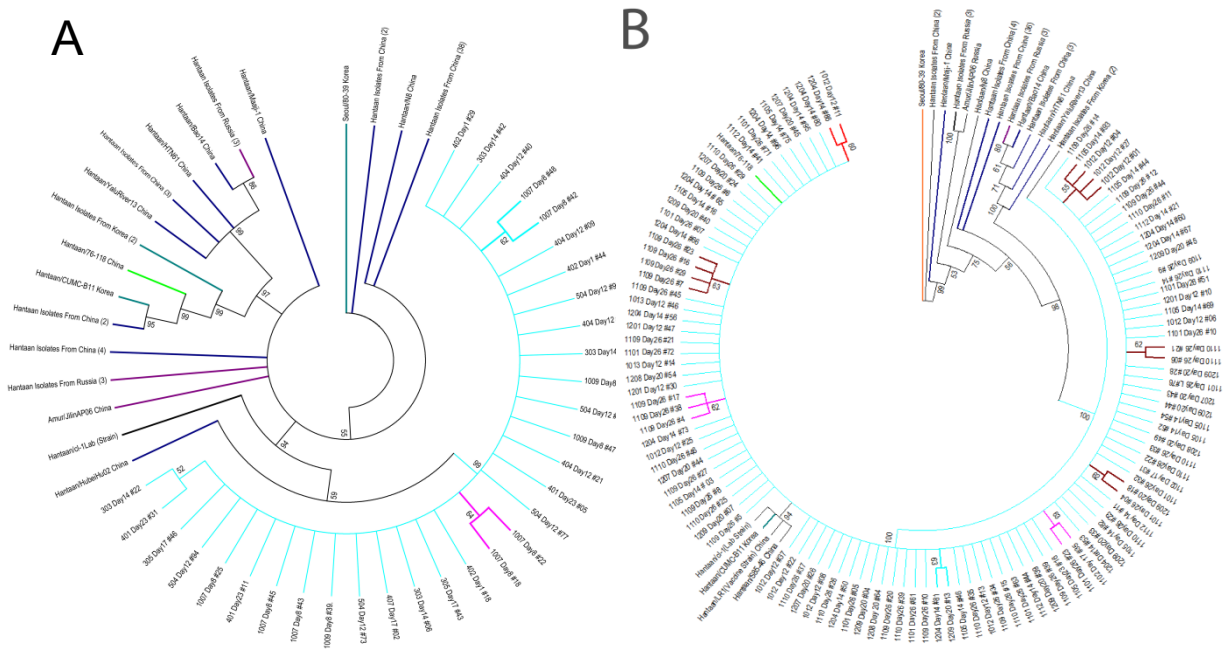

Figure 8. Maximum likelihood phylogeny of the open reading frame of the S-segment and wild type HTNV sequences. Phylograms of nucleotide sequences from mock-treated (**A**) and ribavirin-treated (**B**) HTNV-infected mouse lungs. The evolutionary history was inferred by using the Maximum Likelihood method based on the Tamura-Nei model [157]. The tree with the highest log likelihood is shown for each data set. Initial tree(s) for the heuristic search were obtained automatically by applying Neighbor-Join and BioNJ algorithms to a matrix of pairwise distances estimated using the Maximum Composite Likelihood approach, and then selecting the topology with superior log likelihood value. The tree is drawn to scale, with branch lengths measured in the number of substitutions per site. The analysis involved 180 nucleotide sequences. Codon positions included were 1st+2nd+3rd+Noncoding. All positions containing gaps and missing data were eliminated. There were a total of 1233 positions in the final dataset. Evolutionary analyses were conducted in MEGA 5 [154].

Ratio of nonsynonymous to synonymous substitution rates

Intrahost genetic variation of RNA viruses arises due to their intrinsically high mutation rates, resulting from error-prone replication (i.e., a lack of proofreading polymerase activity). It is constrained by purifying selection (also called negative selection), which eliminates new mutations that reduce specific infectivity relative to that of the ancestral sequence, for example, by decreasing the ability of an organism with a particular genotype to enter or replicate in a cell. Selection can also favor new genetic variants, as occurs, for example, *in vivo* when novel sequences allow escape from the host's immune response. Such selection favoring new variation is called positive selection. Whether or not selection is acting on a sequence and, if so, what type of selection is present can be detected by comparing the ratios of nonsynonymous to synonymous substitution rates (the *dN*/*dS* ratio).

To test for evidence of sites under positive or negative selection among sequences from mock- and ribavirin-treated, HTNV-infected mice, the coding regions of the nucleotide sequences were aligned using ClustalW and analyzed using the Datamonkey web-based interface to the SLAC, FEL, IFEL, and FUBAR programs [119, 120]. Each of these models uses different approaches to estimate the rates of *dN* and *dS* at each site. For example, SLAC is a counting method that may lack power for data sets comprising a small number of sequences or low divergence, such as in the mock-treated group [158], but it was included for comparison. Fixed-effects models such as FEL and iFEL directly estimate *dN* and *dS* at each site, in external and internal branches, respectively.

The FUBAR method estimates the alignment-wide distribution of synonymous (α) and nonsynonymous (β) substitution rates, whose ratio (ω) is a common measure of the type of natural selection operating on the gene (ω values of <1 are interpreted as representing purifying selection, ω values of >1 represent pervasive diversifying selection, and ω values not statistically different from 1 represent neutral evolution) [119, 120]. Having obtained this surface via Markov chain Monte Carlo sampling, it is then possible to apply an empirical Bayesian procedure to estimate the posterior distribution of ω at a given site, and thus to determine which sites are constrained and which ones are evolving adaptively.

The SLAC method did not detect any codons under positive or negative selection for either the mock- or ribavirin-treated group. FUBAR analyses detected three codons under pervasive purifying selection in the mock-treated group (codons 37, 193, and 225), and FEL analyses found the same three codons under negative selection in the mock-treated group (codons 37, 193, and 225). FEL also found, for the ribavirin-treated group, that codons 71 and 224 had two negatively selected sites. The iFEL and FUBAR analyses of the ribavirin-treated group (**Table 5**) found two sites with positive selection (A410 and P248) and two sites with pervasive diversifying selection (F165 and P248).

To explore the potential for episodic selection or a small number of branches subject to positive selection, we used MEME [159]. MEME models variable ω values across lineages at an individual site (i.e., each site is treated as a fixed-effects component of the model). These analyses (**Table 5**) revealed two

codons with episodic selection (F165 and P248) within the ribavirin-treated group, but none within the mock-treated group.

Table 5.

Summary of MEME, IFEL and FUBAR analyses

	Amino acid identified→	F165	A410	P248
MEME[1]	**α**	$5x10^{-6}$	0	n.d.
	β	0	0	n.d.
	β+	10000	3627	n.d.
	p-value	$9.88x10^{-7}$	0.0708	n.d.
IFEL	***dS***	N/A	$5x10^{-9}$	$5x10^{-9}$
	dN	N/A	78.60	95.09
	dN/dS	N/A	15720120000	19017460000
	p-value	N/A	0.036374	0.0293944
FUBAR[2]	**α**	0.504806	n.d.	0.363532
	β	4.97696	n.d.	2.63544
	β >α	0.943738	n.d.	0.901973
	Emp. Bayes factor	17.7	n.d.	9.7

Legend: n.d.-none detected; [1]episodic diversifying selection, p-values based on Simes' procedure (0.1 significance level); [2]Pervasive diversifying selection at a posterior probability ≥0.9.

Discussion

Infection of hantaviruses can lead to persistence in one host without disease (rodent reservoir), acute infection with rapid clearance in another host (adult laboratory mice or wild, non-reservoir rodents), or lethal disease in yet another (humans or suckling mice). Upon accidental infection of humans, hantaviruses may cause two different illnesses in humans: HFRS and HPS [8, 15, 160]. At present, there are no vaccines or antivirals available by the FDA for treatment of either disease. However, intravenous ribavirin has been used in clinical studies in China and Korea [130] for treatment of HFRS and HPS ([161, 162]. While the studies with HFRS show promise for ribavirin as a therapeutic approach, its use in treatment of HPS is as yet inconclusive. Efficacy studies in the lethal HPS hamster model of ANDV infection suggest that it does have potential [163]. Understanding ribavirin's mechanism of action and potential for selecting for drug resistance *in vitro* and *in vivo* is important to a full interpretation of its efficacy and safety for treatment of diseases caused by hantaviruses.

In this study, we employed a lethal murine model of hantaviral disease with a prototypic HFRS virus, HTNV, to gain insight into viral replication and genetic variation over time with and without ribavirin treatment. Our research and that of others have shown that small molecules such as ribavirin increase the mutation load of the viral genome, which results in the extinction of the virus *in vitro* [135, 144-147, 151]. Improving our understanding of how to drive a virus to extinction by increasing genetic variation by use of small antiviral molecules such as ribavirin (e.g., lethal mutagenesis) requires insight into how viruses evolve and

adapt within different environments. In naturally occurring infection cycles, changes in the standing genetic variation of viruses can arise during within-host (e.g., immune pressure, replication, and diversification) and between-host (e.g., transmission bottlenecks) processes of infection. Given the large population sizes and high mutation rates of RNA viruses, they are predicted to be enormously effective in their evolutionary response to natural selection. However, RNA viruses rarely show adaptive, positive selection in nature. This may be due to theoretical and experimental findings that suggest that many RNA viruses have evolved to replicate near their mutation threshold and hence have a relatively limited ability to explore the mutational space required for adaptation. Hence, the concept emerged to use mutagen-increasing small molecules such as ribavirin to increase the mutation load and cause error catastrophe or lethal extinction of the virus [135, 164-167]. Error catastrophe is defined as a loss of genetic fidelity during RNA virus replication that results in a lethal accumulation of errors. Ribavirin increases the level of genetic variation or mutation load in hantaviruses, polioviruses, and others in the presence of ribavirin *in vitro*, resulting in error catastrophe or lethal extinction once a specific level of mutation is achieved by the drug [135, 144-147, 151]. Therefore, one might predict that coupled with normal within-host selection processes, ribavirin would be even more effective in causing error catastrophe or lethal extinction of the virus *in vivo* than *in vitro*.

Our studies showed an elevation in mutation frequency of HTNV S-segment sequences in mice treated with ribavirin similar to that we previously

reported for our *in vitro* studies [151, 152]. We observed a corresponding decline in specific infectivity of HTNV over the course of infection in the ribavirin-treated mice, but we also observed a similar decline in untreated mice (**Figure 4**). The biological bases for each were clearly different, since in the ribavirin-treated, HTNV-infected mice, we noted an increased mutational load and positive selection, while in the untreated mice, we observed a decreased mutational load and purifying selection (**Tables 3** to **5**). Hence, while the difference in phenotype of the populations showed only a marginally significant *P* value (**Figure 4**), significant changes occurred in the adaptation of the virus within the N protein (**Table 5**), in one evolutionary step (**Figure 8B** versus **Figure 8A**). Overall, the population data are consistent with the changes in selective infectivity (ability of a transcribed poliovirus RNA to produce infectious virus) reported for poliovirus in a direct test of the importance of mutation load *in vitro* [145]. In that study, the ability of poliovirus RNA to produce infectious virus decreased with increased mutations, and the phenotype became lethal at a specific mutation load. Intriguingly, we found a decrease in diversity of the vRNA population in the untreated, HTNV-infected mice, rather than an increase in genetic diversity or selection of individual adaptive mutations that correlated with enhanced pathogenesis in the suckling mouse model.

We have few studies to compare our data with regarding the evolution of viruses in animal models of infection where animals are treated with ribavirin. Vignuzzi et al. reported an increase in genetic diversity which correlated with increased pathogenesis of poliovirus in a mouse model treated with ribavirin

[147]. Studies with foot-and-mouth disease virus (FMDV) showed that ribavirin-induced mutagenesis of an FMDV population *in vitro* resulted in attenuation of pathogenicity when these viruses were assessed by infection of an *in vivo* mouse model [168]. Recently, coxsackie virus B3 has been shown to have a lower mutational robustness (greater sensitivity to ribavirin) than that of poliovirus [169]. While direct comparison of the mutational robustness of HTNV to the values reported for poliovirus and coxsackie virus B3 is not possible, the values obtained *in vitro* and in this study are probably similar to or higher than those for poliovirus. The differences in the trajectories of these viruses may reflect unique solutions in their biological and evolutionary strategies for survival and adaptation during infection. For example, in contrast to hantaviruses, polioviruses have only one reservoir, humans, to maintain their reproductive rate, and FMDVs are maintained among cloven-hoofed animals as reservoirs. Among hantaviruses, human-to-human transmission has never been observed for HTNV and has been observed only for ANDV, which is endemic in South America.

In addition to an elevated mutation load in ribavirin-treated mice, the average branch length is much longer in our phylogeny for ribavirin-treated, HTNV-infected mice (**Figure 9B**) than in that for mock-treated mice, indicating that the changes induced by ribavirin can trigger longer evolutionary pathways. Numerous gain- or loss-of-negative-charge substitutions were revealed within the N protein (**Table 4**) and propagated in the sequence pool, suggesting a selective pressure of amino acids in the presence of ribavirin. Signatures of adaptation in these populations, while preliminary, suggest the importance of the viral N

protein in the adaptive process. This is not surprising, since N is multifunctional and may interact with at least three host proteins. The N protein has the ability to interact with host cellular proteins to modulate immune signaling [107] and apoptosis [106]. The N protein interacts with several host cellular proteins, such as Daxx, a Fas-mediated apoptosis enhancer [170], the ubiquitin-like modifier (SUMO-1), and ubiquitin-conjugating enzyme 9 (Ubc9) [171]. The precise mechanism associated with these interactions involving N in the life cycle of the virus is as yet unknown.

HTNV populations from mock-treated and ribavirin-treated mice followed two different types of evolutionary trajectories, evolving under purifying and positive selection, respectively. Because our data indicate that virus populations in ribavirin-treated hosts have greater diversity, there are two non-mutually exclusive potential reasons for this difference. First, the difference in trajectories could be influenced by changes in selection experienced by the virus that were caused by ribavirin. For example, ribavirin may change the nature of the mouse immune response, resulting in different alleles, not present in the ancestor, being favored when HTNV finds itself in a ribavirin-treated host. Second, the difference in trajectories could be influenced by ribavirin's documented effect on the supply of new mutations. Increased mutation rates generated by exposure to ribavirin may give HTNV access to new, perhaps rare, alleles that would be beneficial in both treated and untreated hosts. Such universally beneficial alleles may exist because the HTNV used in this study is naive with regard to this suckling mouse model and may be far from its potential genetic optimum in this host. Regardless

of the underlying selective cause, our experiments suggest that although the viruses within the ribavirin-treated, HTNV-infected mouse virus populations may suffer from a greater proportion of deleterious mutations, they harness the increased mutation rate to also achieve genetic changes that improve their survival over that of the wild type when exposed to a host treated with ribavirin.

In conclusion, the data presented herein suggest that ribavirin promotes a hypermutable environment that increases the mutation load in HTNV sequences in mice. Intriguingly, the levels of vRNA were similar in untreated and treated HTNV-infected mice, which suggests a potential benefit of increased mutational loads. Furthermore, the positive selection of amino acids in the N protein in the ribavirin-treated mice, but not the untreated mice, implies that ribavirin can also change the rate of adaptive evolution. In other words, sequence space not obtainable in untreated, HTNV-infected mice becomes available with ribavirin. With the increased availability of next-generation sequencing and reduced costs, future experiments will also capture other segments of the HTNV and hold promise to provide additional insights into evolutionary trajectories of additional virus-host interactions (entry-glycoprotein and polymerase-replication interactions). Experimental models of RNA viral evolution have largely been conducted within continuous cell lines in which viruses are well adapted and by creation of selection with temperature changes or small-molecule inhibitors of replication. *In vivo* approaches are a critical next step toward validation of these findings and to define the molecular mechanisms that influence zoonotic virus evolution and adaption in spillover hosts. In the specific case of ribavirin, the *in*

vivo mouse model revealed positive selection of amino acids, while the *in vitro* studies did not. Future efforts will continue to explore the mechanisms of selection and adaptation of *Hantavirus in vivo* to not only promote an understanding of how to drive lethal extinction therapeutically but also provide insight into the molecular mechanisms that influence zoonotic virus evolution and adaption in reservoirs or spillover hosts.

CHAPTER III

A NEW PRIMARY LUNG MICROVASCULAR ENDOTHELIAL CELL CULTURE MODEL FROM DEER MOUSE TO STUDY NEW WORLD HANTAVIRUS INFECTIONS

Introduction

Hantaviruses persistently infect a variety of rodent, mole, vole, shrew, or bat species with no apparent illness or pathology [8, 65]. Only the rodent-borne hantaviruses cause disease in humans, although, not all cause disease. The New World hantaviruses that are associated with HPS have ≤50% mortality, while Old World hantaviruses that cause HFRS have a mortality ranging from 1-12% [8]; neither disease has vaccines for prevention or antivirals for treatment in the United States. In China and Far East Russia, three vaccines are licensed and used for the treatment of HFRS. The three inactivated vaccines were created using purified suckling-mouse brains, golden hamster kidney cells or Mongolian gerbil kidney cells, respectively, and have shown to elicit protective efficacy in approximately 90% of populations vaccinated [172].

At present, there are at least 24 species of hantaviruses that are each harbored by a unique rodent reservoir species. The observed host restriction of rodent-borne hantaviruses is postulated to be due to coevolution over millions of

years [173-175]. To date, the vast majority of *in vitro* studies of infection and mechanism of New World hantaviruses have focused on nonrodent (nonreservoir host) cell lines such as Vero E6 (African green monkey kidney cells) or primary human bronchial epithelial cells. While these studies give valuable insight into interactions of hantaviruses with nonhuman primate and human cells, they are not appropriate for understanding interactions of the hantaviruses with their reservoir, mechanisms of host restriction or persistence in nonreservoir rodents. The availability of a physiologically and genetically relevant *in vitro* model is particularly important given the millions of years of coevolution that allow persistence of hantaviruses without disease. The availability of rodent reservoir models will provide an important resource to advance our understanding of hantavirus-reservoir host interplay that results in modulation of host reservoir signaling pathways results in immune suppression and persistent infection.

The International Committee on Taxonomy of Viruses (ICTV) recognizes 24 species within the genus, *Hantavirus*, from rodents, bats and shrews. Of these 24, 19 have been isolated; the vast majority of these isolates have been from the lungs of wild rodents [113, 176, 177], and more recently, from human tissue using Vero E6 cells [113, 176, 177]. In addition to serving as a vehicle for isolation of hantaviruses, Vero E6 cells have also been widely used in the propagation and study of hantaviruses. Recently, research published by Dr. Jonas Klingström shows that embryonic fibroblast cells from voles can be used to isolate and propagate PUUV [178]. This is an important advancement since none of the Vero E6-derived HFRS isolates *Hantavirus* have been shown to cause

disease similar to humans in any animal model, including nonhuman primates. Severe disease has only been demonstrated through intracranial inoculation of newborn 1 day old mice with HTNV [179].

In 2006, Hooper published the first model of HPS disease in the Syrian hamster using ANDV [131]. It is unknown at present what genotypic/phenotypic or protein function that ANDV has as compared to other hantaviruses that recreate disease. One potential difference of ANDV is that it is the only member of the *Hantavirus* documented to transmit person to person [180]. Therefore, we may reason that ANDV has evolved with less host restriction. In other words, ANDV may acts more like a generalist than a specialist species, perhaps allowing it to be isolated in Vero E6 cells without a loss in its virulent phenotype (in humans). Even so, ANDV was not virulent in nonhuman primates [181]. Several studies have shown that RNA viruses undergo genetic changes when they spillover into new host environments and that a virus's fitness in one environment may not always extended to a different environment, *in vitro* or *in vivo* [182-185]. Understanding how these viruses persist in their rodent reservoir and adapt to new rodent hosts will provide new insight into why and how hantaviruses suppress disease in one host yet elicit disease in others. Moreover, advancements in discovery of antiviral therapeutics and vaccines depend on better animal models that resemble human disease.

Fortunately, in the past decade the deer mouse, *Peromyscus maniculatus*, has gained momentum as a model for several areas of research leading recently, to the complete sequencing of its genome [186]. For the New World hantaviruses

the deer mouse has been an important model for the study of SNV infection and host immune responses. Deer mice infected with SNV have detectable levels of viral antigen at 5 days post-infection peaking at day 15 in the lung along with vRNA levels, with no mice showing clinical signs of HPS [81]. SNV infections of deer mice show chemokine and cytokine repression throughout the course of infections in the lung, whereas, the spleen showed a significant (p<0.05) increase in TGFβ and CCL2 (diphasic) and, IL-12, IL-21, IL-23 and CCL5 [81]. Persistent SNV infections of deer mice have been shown to promote a Treg phenotype by expression of Fox-p3 and suppression of T-bet and GATA3 (Th1 and Th2 genes) [91]. The Treg profile was suggested to be due to an increase in TGFβ, whereas the acute infection showed increases in INFγ and IL-5 [91]. Dr. Sabra Klein's laboratory has demonstrated that SEOV infection of primary lung (from Norway rats), results in an increase in TGFβ in alveolar macrophages but not in lung microvascular endothelial cells (L-MVEC) [49]. SEOV infection of L-MVEC infection showed an up-regulation of PD-L1 using western blot but not in alveolar macrophages [49]. PD-L1 promotes an anti-inflammatory immune response by inducing CD^{+4} T cells to Treg cells. In conclusion, these studies show that a persistent infection of hantavirus in their reservoir hosts are promoted by eliciting a Treg phenotype with a down-regulated immune response [81, 91].

The lung endothelium is the primary site for hantavirus replication following infection of the lung in reservoir and nonreservoir host species. We chose to use L-MVEC to build a physiologically relevant *in vitro* model of the rodent reservoir host. Herein, we report the successful isolation and culture of

primary L-MVEC from deer mice, the reservoir for SNV. We show that L-MVEC retained expression of the endothelial specific surface receptors, ICAM-2, over eight passages. We also report the infection of the deer mouse L-MVEC with SNV, SEOV and BCCV and the cytokine and chemokine expression levels after infection. Although preliminary, SNV, SEOV and BCCV induced a TGFβ immune response during infection of deer mouse L-MVEC albeit at different levels.

Materials & Methods

Viruses and deer mice

All viruses were propagated in Vero E6 cells using DMEM (10% FBS, 1% Pen/Strep and 5 mM L-Glutamine). Viruses used in this study: SNV strain Convict Creek 107 (CC107, Dr. Jay Hooper, USAMRIID), SEOV strain SR-11, (Dr. Connie Schmaljohn, USAMRIID) and BCCV (Dr. Christina Spiropoulou, CDC). Deer mice (*Peromyscus maniculatus)* were provided by the National Institute of Health's (NIH) Rocky Mountain Laboratory. All animals were euthanized upon arrival at University of Louisville's Clinical Translational Research Building (CTRB) vivarium. All *in* vivo procedures were conducted in accordance with an approved institutional animal use protocol from University of Louisville's IACUC.

Isolation and culture of lung microvascular endothelial cells (L-MVEC) from deer mice

A protocol was developed to isolate L-MVEC based on methods outlined by Hartwell et al., 1998 (**Figure 9**) [187]. Rodents were euthanized by CO_2 asphyxiation and their lungs were excised and placed in transport media (DMEM, 1% penicillin/streptomycin). Lungs were then removed from media and minced into small pieces using two scalpels. Minced lung pieces were digested in 0.5 mg/mL collagenase A (Sigma) for 1 hr at 37°C, shaking every 15 min. After incubation, the lung digest was first triturated using a 10 mL syringe (with no needle) then filtered through a 70-100 μm cell strainer. The filtered cells were centrifuged twice at 100 x *g* for 10 min at 4°C, resuspended in 5 mL of Complete Endothelial Cell Culture Media (M1168 media) (Cell Biologics) and plated on a 100 x 20 mm tissue culture dish (CytoOne) (passage 1) coated with 0.2% Matrigel (BD Biosciences). After incubating for two days at 37°C and 5% CO_2, cells were incubated with a rabbit polyclonal antibody against mouse ICAM-2 (Fitzgerald) bound to magnetic anti rabbit Dynabeads (Invitrogen). ICAM-2 is a type I transmembrane glycoprotein found in tight adhesion junctions of endothelial cells. ICAM-2-positive cells were purified by magnetic separation and washing with Dulbecco's phosphate-buffered saline (DPBS), without Ca^{2+} and Mg^{2+}, followed by seeding on a 0.2% gelatin-coated dish (**Figure 9**). The L-MVEC were subcultured, using 0.25% Trypsin EDTA, at a ratio of 1:2 or 1:5 and seeded onto 0.2% gelatin-coated dish every 2-3 or 3-4 days, until they reached 85% confluence.

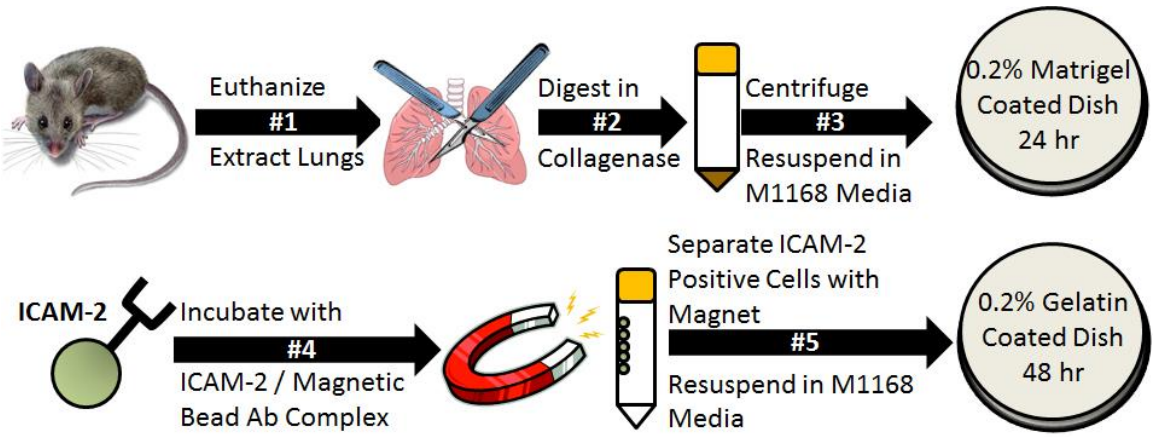

Figure 9. Illustration of method for isolation of deer mouse L-MVEC. Five main steps for isolation of L-MVEC from deer mice. Deer mice L-MVEC were isolated in five steps as follows: (**1**) Euthanize mice using CO_2, extract the lung and place in transport media; (**2**) Mince lungs using scalpels and digest minced lungs in collagenase A for 1 hr at 37°C; (**3**) Pass collagenase mixture through cell strainer and centrifuge at 250 x g for 10 min at 4°C, twice; Cells were resuspended in M1168 media and cultured for 48 hr at 37°C, 5% CO_2 on a 100 x 20 mm tissue culture dish, coated for 1 hr with matrigel 0.2%; (**4**) ICAM-2 conjugated bead complexes were created by incubating an ICAM-2 (Fitzgerald) rabbit anti-mouse antibody and a sheep anti-rabbit Dynabead secondary (Invitrogen) overnight at 4°C with rotation, cells were washed and ICAM-2 antibody bead complexes were incubated on cells for 1 hr at 37°C, 5% CO_2 ; Cells were detached from dish using 0.25% Trypsin EDTA for no more than 2 min; (**5**) ICAM-2 positive cells were isolated using a magnet and suspended in M1168 media, three times; Cells were cultured on a 0.2% gelatin-coated dish for 48 hr at 37°C, 5% CO_2.

Fluorescence-Activated Cell Sorting (FACS) analyses

Deer mice L-MVEC were detached from cell culture dishes using 2 mL 0.2% EDTA in DPBS and vigorous pipetting. The resulting cell suspension was mixed with an equal part FBS and volume was increased to 10 mL with DPBS. Cells were washed here, and in subsequent steps, by centrifugation at 250 x *g* for 10 min at 4°C followed by resuspension in DPBS with 2% FBS ("staining buffer"). After two washes in staining buffer, polyclonal rabbit anti-mouse ICAM-2 (Fitzgerald) (1:200) was added to 100 µL cells (10^6 cells) and incubated for 30 min on wet ice. Cells were washed twice as above and resuspended in 100 µL staining buffer. Fluorescent secondary antibody (1:1000) conjugate was added and incubated for 30 min in the dark on wet ice (goat-anti rabbit IgG Alexafluor-647, Molecular Probes). Cells were washed twice as above and resuspended in 4% paraformaldehyde for 15 min at room temperature in the dark. Cells were centrifuged and resuspended in 0.2 mL DPBS for analysis on a FACSCalibur flow cytometer (BD Biosciences). Single-stained controls were used for compensation. Data was analyzed with FlowJo (TreeStar, Inc.). Control cells treated with secondary antibody-alone were used to set the positive population gate.

Infections and treatment of L-MVEC

Deer mice L-MVEC were seeded in a 6-well plate at 1.75 x 10^5 cells per well for 24 hr prior to infection (80% confluence after 24 hr). L-MVEC were washed with DPBS and infected with 100 µL of Vero E6-derived SNV (CC107) at

a MOI of 0.06 (1 x 10^5 PFU/mL) or treated with LPS (3.33 µg/mL) for 1 hr at 37°C, 5% CO_2. After infection, 2 mL of M1168 media was added to each well and infections were allowed to proceed for 48 hr at 37°C with 5% CO_2. After 48 hr the cell culture supernatant, cellular RNA, and cellular protein were collected.

Western blots

Total protein was isolated from deer mice L-MVEC as follows. Cellular proteins were isolated using Trizol and dialyzed in 0.1% SDS for 23 hr in 10 kDA molecular weight dialysis tubing. The protein precipitate was suspended in 8 M urea in Tris-HCl, pH 8.0 in aqueous 1% SDS and aliquoted/stored at -80°C until analysis. Proteins were separated by 12% Sodium Dodecyl Sulfate (SDS) Polyacrylamide Gel Electrophoresis (PAGE) and transferred to nitrocellulose or nytran. Membrane was blocked in 5 mL of blocking solution (5% dry, low fat dry milk in 1X TBST) and incubated with polyclonal antibody made to SNV N protein in rabbit (1:500) and polyclonal antibody against calnexin made in rabbit (Abcam) (1:1000). Primary antibody was detected by incubation with goat anti-rabbit polyclonal horseradish peroxidase (HRP)-conjugated secondary antibody (Abcam) (1:2000) for 1 hr at RT in the dark. Visualization of bands was conducted using Chemiluminescent HRP substrate (ECL, Invitrogen) followed by exposure to autoradiographic film.

Plaque assay

Six-well plates were seeded with 3 x 10^5 Vero E6 cells per well and incubated at 37°C, 5% CO_2 for 3 days, until confluent [188]. Wells were infected in duplicate or triplicate with 10-fold serial dilutions of supernatant from deer mouse infected L-MVEC. Virus and cells were incubated for 1 hr at 37°C, 5% CO_2, with rocking every 15 min. After infection, 2 mL of 1.6% SeaKem Agar (Cambrex) was added to each well and plates were allowed to incubate upside down in a foil-covered humidity chamber for 7 or 10 days at 37°C 5% CO_2. A second SeaKem agar containing 5% neutral red solution (Sigma) was added for New World viruses (SNV and BCCV) on day 7 post infection and day 10 for Old World viruses (SEOV). Plates were again incubated in a foil-covered chamber upside down at 37°C, 5% CO_2 for the remaining 3 days. Plates were observed for plaques twice a day for 3 days after the neutral red agar overlay.

Virus cell-based ELISA

96-well plates of nearly confluent Vero E6 cells, seeded at 20,000 cells per well and grown at 37°C, 5% CO_2 for 3 days, were infected with 2-fold serial dilutions of supernatant from deer mouse virus-infected cells and incubated for 3-4 days. After three days, cells were fixed with acetone and methanol (1:4) and blocked with 5% nonfat milk in DPBS. Human convalescent serum was added to 5% nonfat milk in DPBS and used to identify cells expressing N protein (1:500) for 1 hr at RT. The primary antibody was detected with a secondary anti-human HRP-labeled antibody. Plates were developed using substrate 2,2'-Azino bis [3-

ethylbenzothiazoline-6-sulfonic acid]-diammonium salt (ABTS) (KPL) for 30 min at RT in the dark and read using a Synergy 4 microplate reader (BioTek) at 405 nm.

Relative expression levels of cytokines, chemokines and quantification of viral RNA by qRT-PCR

Total cellular RNA was extracted from L-MVEC supernatants using Trizol (Invitrogen) according to the manufacturer instructions. 1 µg of RNA along with random hexamer primers were used for cDNA synthesis by Superscript III Reverse Transcriptase (Invitrogen). For real-time PCR, we used SYBR green master mix (Invitrogen) and performed reactions in duplicate using 3 µL of cDNA (33 ng/µl) and a 10 µM of each primer (final concentration 1 µM) in a 10 µL total reaction volume. Sequence-specific primers used to amplify SNV S-segment genes were (forward: [5'-GTC TTT GCA TGT GCT CCT GA-3'] and reverse: [5'-ATC CCC ATT GAC TGA GTT CG-3']). Primers used to assess cytokine and chemokine expression levels were as published by Schountz et al. (**Table 6**) [81]. The RT-PCR consisted of 1 cycle of 50°C for 5 min and 95°C for 2 min and 40 cycles of 95°C for 30 sec, 60°C for 30 sec using the 7900 Fast Real-Time System (Applied Biosystems) and data analyzed using SDS Software version 1.4.0. The threshold was automatically set by the instrument and Ct determined. Viral RNA and chemokine and cytokine mRNA was quantitated using the mean of the change in Ct values (ΔCt) normalized to the Ct values of glyceraldehyde-3-phosphate dehydrogenase (GAPDH) for each sample ($2^{-\Delta\Delta Ct}$).

Table 6

Primers to assess cytokine and chemokine expression levels

	Forward	Reverse
TGFβ	5'- CGT GGA ACT CTA CCA GAA ATA CAG C -3'	5'- TCA AAA GAC AAC CAC TCA GGC G -3'
IL-6	5'- GGA GTG GTC GAG AAC CAA GA -3'	5'- CAG TGA GGA ACG TCC ACA GA -3'
IL-10	5'- TTA GGG TTA CCT GGG TTG CCA AG -3'	5'- CAA ATG CTC CTT GAT TTC TGG GC -3'
INFγ	5'- ATG CCT TGA AGG ACA ACC AG -3'	5'- CAT GAA GTC GTC CCG TTT CT -3'
CCL2	5'- CAG ACG TAC ACA AGA AAA CTG GAC C -3'	5'- GTC AAG TTC GCA TTC AAA GGT GC -3'
CCL3	5'- AGG AAC CCA GAA ACC TCC AT -3'	5'- CAG CAA ACA GCT TGC AGA AG -3'
GAPDH	5'- GGT GCC AAA AGG GTC ATC ATC TC -3'	5'- GCA GGA AGC GTT GCT GAT AAT CTT G -3'

Results

Isolation and culture of deer mouse L-MVEC.

To achieve insight into the evolution of host switching, I have established (1) a cell culture model of deer mouse L-MVEC, (2) techniques to infect and measure SNV and SEOV replication and (3) techniques to measure the production of infectious particles and host immune responses. Primary L-MVEC from deer mice were isolated from whole lung extract (digested using collagenase) using ICAM-2 dynabead conjugated antibody complex (**Figure 10**). Isolation of primary deer mice L-MVEC into a 100 x 20 mm dish required 3 deer mouse lungs from males at 8-12 weeks of age. ICAM-2 positive L-MVEC were isolated from whole lung extract using magnetic separation. M1168 media was used to propagate the primary L-MVEC and contains supplements and growth factors specific for L-MVEC.

Culture conditions were optimized for the L-MVEC model by testing different flask sizes (T_{75}, T_{25} and 100 x 20 mm dish), cell passaging ratios (1:2 or 1:5), plate coating solutions and different cell culture media. Specifically cells were subcultured at a ratio of 1:2 or 1:5, after cells reached 80% confluence. Morphologically, no changes or loss in the cell number were observed with these two passaging ratios. We further optimized L-MVEC growth conditions by comparing culture dish coating methods. We compared growth on dishes coated with 0.2% Matrigel compared with 0.2% gelatin culture flask; and we noted no morphological differences. To test for potential differences in growth media, we grew L-MVEC in M1168 media, complete DMEM (10% FBS, 1%

Penicillin/Strptomycin, 5 mM L-Glutamine), Minimal Essential Medium (MEM), Opti-MEM or Roswell Park Memorial Institute (RPMI) media. All media except M1168 caused the cells to detach. M1168 media contains growth factors, hormones, amino acids (essential and non-essential), as well as other supplements not found in the other media and this media was used in subsequent infection studies.

Characterization of L-MVEC.

Primary cells can lose viability and phenotype overtime. Assuring the presence of cellular receptors can be used to characterize the phenotypic quality of endothelial cells. For endothelial cells, these include ICAM-2, PE-CAM1 and Ve-Cadherin. Deer mice L-MVEC, at passage 8, were assessed for their ICAM-2 receptor phenotype using FACS.

L-MVEC were detached from the culture dish using 0.2% EDTA. Cells were incubated with an ICAM-2 primary antibody and an Alexaflour 647 secondary for detection. FACS analysis of deer mouse L-MVEC showed two fluorescent peaks ICAM-2 positive peaks (**Figure 11**). The two peaks represented by the red line are ICAM-2 positive L-MVEC and the grey region represents single-stained control cells. The two peaks may be due to; 1) high and dim populations of staining due to the possibility of more or less secondary antibody staining per cell, or 2) a high level of background (represented by the peak in the middle). Single-stained cells were used as controls for the FACS analysis (represented by the grey shaded peak in **Figure 11**). In summary, these

experiments demonstrated that we are successfully able to isolate and propagate deer mice L-MVEC with an ICAM-2 phenotype for 8 passages (**Figure 11**).

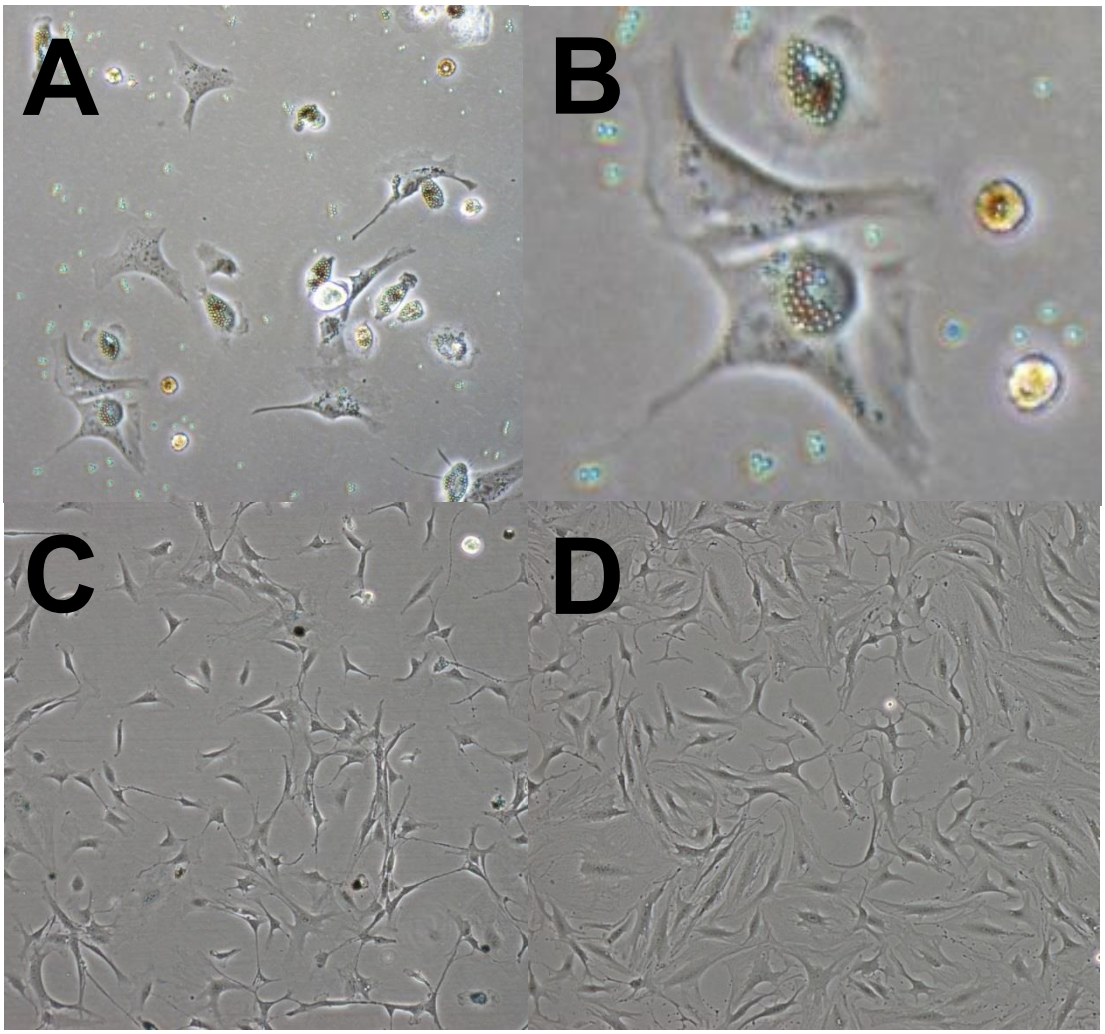

Figure 10. Deer mouse L-MVEC. (A & B) Images of deer mouse L-MVEC using phase contrast. Images were taken 24 hr after bead purification (Passage 2) at 400x magnification (McAllister and Jonsson unpublished data). Dynabeads can be seen as green dots. **(B)** Blown up lower left region of **A**. **(C & D)** Passage 4 and passage 8 –LMVEC at 100x magnification. **(C)** L-MVEC 24 hr post passage 4, at approximately 50% confluence. **(D)** L-MVEC 48 hr post passage 8, at approximately 85% confluence.

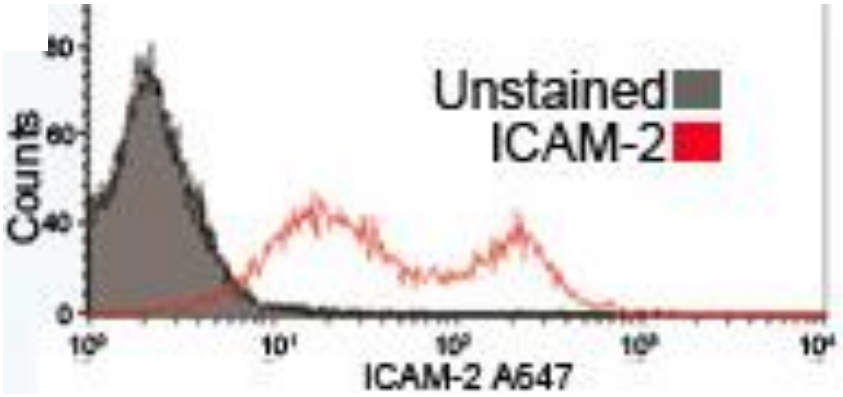

Figure 11. FACS analysis of deer mouse L-MVEC. Passage 8 deer mouse L-MVEC.). FACS analysis using a rabbit anti-mouse ICAM-2 primary antibody (Fitzgerald Cat. # 70R12192) (McAllister, Camp, and Jonsson unpublished data). Single stained control L-MVEC are represented by the grey peak whereas, ICAM-2 labeled L-MVEC are represented by the red line. The red line forms two peaks indicating two populations of ICAM-2 positive stained cells, which are either representing background unspecific staining or cells are tagged with multiple antibodies to ICAM-2 or multiple secondary antibodies are binding to the primary.

Permissiveness of deer mouse L-MVEC to SNV hantaviral infection.

Deer mice L-MVEC were infected with Vero E6 propagated SNV (veSNV) to determine the level of infectious SNV produced from infection and to determine the amount S-segment replication and N protein translation. The S-segment encodes for the N protein which is the most abundant produced by hantaviruses. L-MVEC were infected at a MOI of 0.06 with veSNV for 1 hr in 6-well plates. After infection, 2 mL of M1168 media was added to each well and the plates were incubated for 48 hr at 37°C, 5% CO_2. Supernatant was harvested and stored at -80°C. Total cellular RNA and protein was collected using Trizol (Invitrogen) according to the manufacture.

Total cellular RNA was isolated from L-MVEC using Trizol according to the manufacturer and cDNA was synthesized using random hexamer primers. SNV S-segment specific primers were used for SYBR green qRT-PCR using 100 ng of cDNA, in which primers were designed to generate a ~100 bp qRT-PCR product. SYBR green qRT-PCR was used to assess the amount of replication of SNV in deer mouse L-MVEC by measuring viral S-segment synthesis using the $C_T 2^{-\Delta\Delta Ct}$ method [148, 151]. We found that SNV S-segment RNA levels were 204-fold greater in veSNV infected deer mouse L-MVEC as compared to mock (M1168 media)-infected. We can conclude that the primers from SNV are effective for qRT-PCR analysis, as SNV S-segment has been shown to be increased ~200 fold compared to mock-infected L-MVEC cells (**Figure 12**). GAPDH was measured as an endogenous control to standardize cDNA levels using SYBR green (**Figure 12**).

Western blot was employed to determine if SNV N protein was being translated in the deer mouse L-MVEC. Calnexin was used as an internal cellular marker and loading control. Our method for extracting cellular proteins was effective due to the presence of the N protein and calnexin, an endoplasmic reticulum marker expressed in all cells (**Figure 13**). We have shown that SNV S-segment was expressed and N protein was present in SNV infected deer mouse L-MVEC using Western blot (WB) (**Figures 12 & 13**).

Supernatant from veSNV-infected deer mice L-MVEC cells was assessed for the presence of SNV using plaque assay and cell-based ELISA. Serial 10-fold dilutions of deer mouse L-MVEC SNV supernatant were created to infect Vero E6 cells in duplicate in a 6-well plate, for 1 hr. After infection, SeaKem agar overlay was added over the cells to inhibit spread of virus to cells other than neighbors and plates were incubated for 7 days upside down in a humidity chamber. After 7 days of incubation a neutral red (Sigma) agar was added to each well for visualization of plaques over 3 concurrent days. The seed stock, veSNV, was also quantified to determine if the seed had lost infectivity.

Plaque assays showed no production of SNV in deer mouse infected L-MVEC. Viral titers may have been probably below detection of the plaque assay, given the presence of S-segment RNA and N protein (**Figure 12 and 13**). One possible explanation for the lack of visible plaques may be that the viruses were infecting but not spreading from cell to cell. A second alternative is that the virus was not making plaques. Plaques are not caused by lysis of cells (for hantavirus)

but rather lower cell growth. Hence, hantavirus may have no effect on slowing the growth of deer mouse L-MVEC SNV.

To further ascertain the presence of virus in cells, a cell-based ELISA was conducted which, also determines the viral titer within the supernatant while not relying on the formation of plaques by cell growth inhibition. A cell-based ELISA used 2-fold serial dilutions of virus to infect Vero E6 cells in a 96 well plate, in quadruplicate, for 3 days. Cells were fixed and stained with primary antibody to N protein and probed with secondary using the HRP substrate ABTS. Absorbance readings were conducted with a plate reader at 405 nm, to quantitate positively-infected wells. Absorbance values of mock-infected wells were averaged and the standard deviation of these wells was determined. Positively-infected cells were identified by having a absorbance value greater than the value determined by the formula: [((Ave. Abs. Mock) + 3)/(std of Mock)]. Using the cell-based ELISA, we saw no levels of detectable infection ($TCID_{50}$/mL) in the deer mouse SNV-infected supernatant (**Table 7**). We also conducted a cell-based ELISA on the veSNV and found that the titer was 1 x 10^2 $TCID_{50}$/mL. This was surprising due to the plaque assay titer of 1 x 10^5 PFU/mL using the same veSNV. We tested additional viruses for their levels of infection in deer mouse L-MVEC. Vero E6 propagated SEOV (veSEOV) and BCCV (veBCCV) titers were determined to be 10^6 and 10^7 PFU/mL, respectively using plaque assay. The titers for the same veSEOV and veBCCV determined using cell-based ELISA were again lower (10^4 and 10^3 $TCID_{50}$/mL). This suggests that assay requires further development or optimization.

Infection of deer mouse L-MVEC was explored using a MOI of 1.0 with veSEOV and veBCCV. At 48 hours post infection (hpi) we harvested supernatant and measure the level of infectious virus particles with a cell-based ELISA with produced 10^2 $TCID_{50}$/mL. Interestingly, as with SNV, we were not able to detect viruses by plaque assay. We do not yet fully understand the difference in titer between the two assays; especially when considering that the plaque assay is able to detect more Vero E6 propagated virus than the cell-based ELISA, but not deer mouse L-MVEC supernatant. One potential explanation is the cell-based ELISA detects proteins in cells and not those that egress. Hence if there was a block in egress or spread we would not see plaques, but we would detect positively stained N antigen using cell-based ELISA. Future efforts will also use immunofluorescence which is more sensitive that the cell-based ELISA.

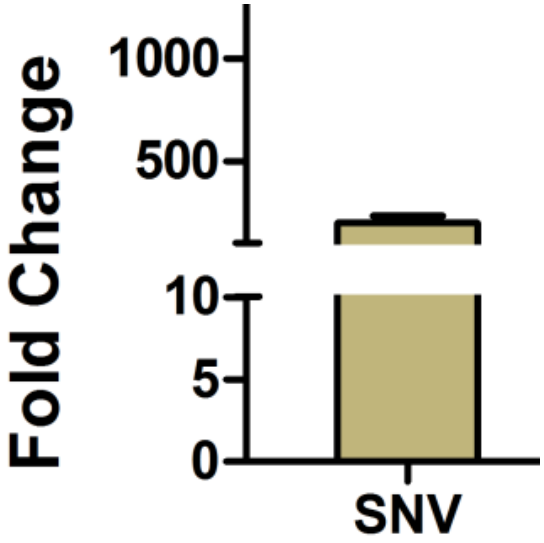

Figure 12. **Viral replication of SNV S-segment in infected primary deer mouse L-MVEC (passage 8).** SYBR green qRT-PCR analysis of SNV S-segment vRNA levels at 48 hpi at a MOI of 0.06 using the comparative $C_T2^{-\Delta\Delta Ct}$ method (McAllister, Gerlach, Jonsson unpublished data).

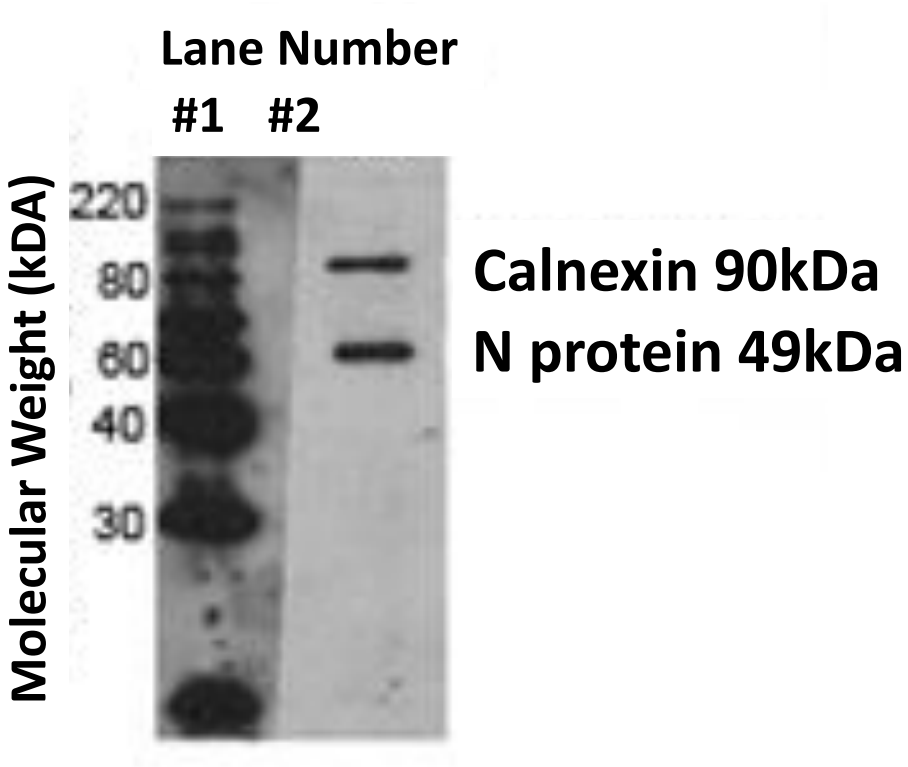

Figure 13. Deer mouse infected L-MVEC WB analysis. Cellular proteins extracted from veSNV (CC107) infected deer mouse L-MVEC, 48 hpi at a MOI of 0.06 (McAllister, Adcock, and Jonsson unpublished data). Proteins were separated by 12% SDS-PAGE, transferred to a nitrocellulose or nytran membrane and visualized by exposure to autoradiographic film using ECL Novex ECL HRP Chemiluminescent Substrate Reagent Kit (Invitrogen).

Table 7.

Cell-based ELISA and plaque assay titers of infected deer mouse L-MVEC at MOIs of 1 and 0.6, 48 hpi and Vero E6 seed stock viruses

Virus	Deer Mouse L-MVEC (48 hpi)	Vero E6
Plaque Assay (PFU/mL) Titers		
SNV (CC107)	Negative	1×10^5
BCCV	Negative	4.6×10^6
SEOV (SR-11)	Negative	2.4×10^7
Mock	Negative	Negative
cell-based ELISA ($TCID_{50}$/mL)		
SNV (CC107)	Negative	1×10^2
BCCV	2.5×10^2	5×10^4
SEOV (SR-11)	1.6×10^2	3×10^3
Mock	Negative	Negative

*Limit of detection 10^2 PFU/mL or $TCID_{50}$/mL

Innate immune signaling profiles mounted by deer mouse L-MVEC when infected with reservoir and nonreservoir hantaviruses

We will probe for cytokine and chemokine responses produced by deer mouse L-MVEC during reservoir and nonreservoir hantavirus infections. Prior studies have shown that during a hantavirus infection of a reservoir host the N protein can inhibit NFκB translocation to the nucleus thus down regulating TNFα-receptor-mediated-signaling (TNFR) and inhibiting a pro-inflammatory state [104, 106, 107]. In human primary L-MVEC ANDV and PHV show a down regulation of INF induced Stat1/2 pathways [101]. Cellular chemokines and cytokines up-regulate both the JAK-STAT pathway and the TNFR pathway. Also, as discussed earlier a reservoir infection with SEOV in Norway rat L-MVEC showed upregulation of PD-L1 which is known to elicit an anti-inflammatory Treg response [49]. Therefore, we predict that during a reservoir infection (deer mouse L-MVEC infected with SNV) we expect inhibition of a pro-inflamatory state, whereas as nonreservoir infection will induce a pro-inflamatory state through the JAK-STAT and/or the TNFR pathways.

Deer mouse L-MVEC were used to assess the immune response during veSNV (reservoir virus), veBCCV and veSEOV viral infections [81]. Deer mouse L-MVEC were infected at a MOI of 1.0 for veBCCV and veSEOV and a MOI of 0.06 for veSNV. Infections were conducted in a 6-well plate for 1 hr. M1168 media was added at a volume of 2 mL per well and the plate was incubated for 48 hr. After infection total cellular RNA was isolated from L-MVEC using Trizol and cDNA was synthesized using random hexamer primers. Using 100 ng of

cDNA SYBR green qRT-PCR was used to assess the amount of cytokine and chemokine mRNA levels in deer mouse L-MVEC using the $C_T2^{-\Delta\Delta Ct}$ method [148, 151]. GAPDH was measured (using published primers) and used as an endogenous control to standardize cDNA levels using SYBR green (**Figure 12**). Published primer sets, by Shountz et al. 2012, specific to the deer mouse were used to assess the immune responses.

Our experiment shows that the deer mouse L-MVEC immune response can be mounted at 48 hpi, after infecting at a MOI of 1.0 for BCCV, and SEOV (SR-11) and a MOI of 0.06 for SNV (CC107) (**Figure 14**). At the time of infection the titer for SNV had yet to be determined so we blindly infected. The positive LPS showed an increase in TGFβ, IL6, INFγ, and CCL2 (**Figure14**). This is what we expected for our positive control, showing that the L-MVEC were capable of mounting an immune response. TGFβ increased during infection by BCCV and SEOV and slightly increased for SNV (**Figure 14**). In contrast to Dr. Klein's results with SEOV, TGFβ increased in L-MVEC during infection by BCCV and SEOV, but not SNV.

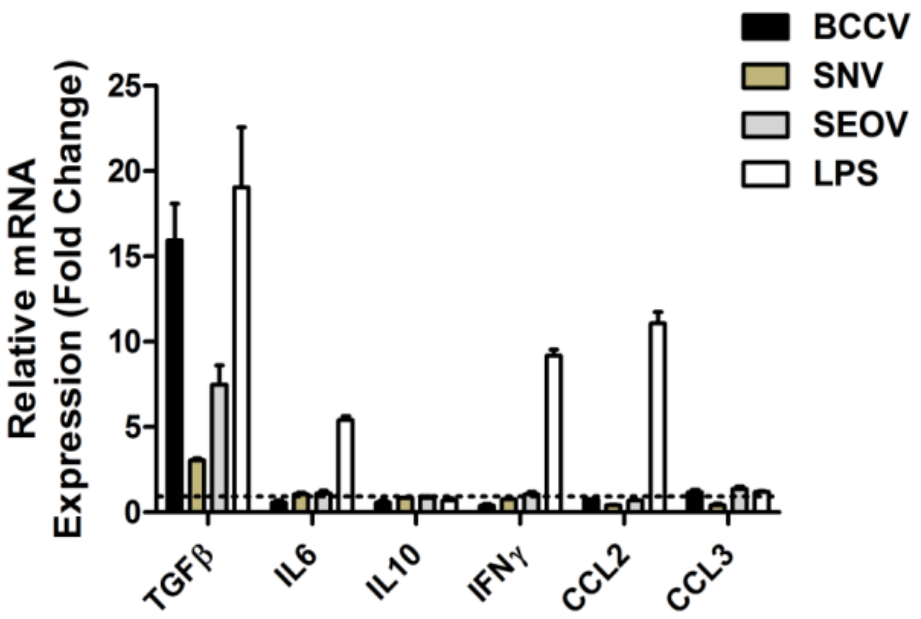

Figure 14. Infected deer mouse L-MVEC innate immune signaling. Gene expression of deer mouse LMVEC (passage 8) after infection with hantaviruses (qRT-PCR). L-MVEC were infected with veBCCV, veSNV (CC107), and veSEOV (SR-11) or treated with LPS (1:1000) for 48 hrs infection at a MOI 1.0 and 0.06 (McAllister, Gerlach, Jonsson unpublished data).

Discussion

My preliminary data has established a system for probing the evolution and signaling pathways of hantaviruses within a natural reservoir model. We have successfully isolated and passaged L-MVEC from deer mice, which maintained ICAM-2 expression and consistent cell morphologies over 8 passages. For the FACS analysis our result for ICAM-2 expression showed two peaks. In order to alleviate the result (two peaks), in the future we will perform titrations of the ICAM-2 antibody to determine the optimal concentration to use. This will either bring down the fluorescence of 1) the peak possibly representing the L-MVEC population that are tagged with multiple secondary antibodies (right red peak) or 2) the middle peak possibly representing L-MVEC population bound by secondary antibody (not expressing ICAM-2).

Further, we optimized culture conditions for the L-MVEC model that allow expansion and growth of the cells for use in future studies. In future studies we will characterize my L-MVEC for the presences of ICAM-2 (CD102), PECAM-1 (CD31) and VE-cadherin (CD144) which are the main surface receptors used to distinguish L-MVEC from other cells [187, 189-191]. PECAM-1 and VE-cadherin are tight intracellular junction surface proteins. It has been shown that vascular leakage of human endothelial cells infected with hantaviruses are negatively-correlated with VE-cadherin surface expression levels [192]. We will probe for ICAM-2, PECAM-1 and VE-cadherin L-MVEC surface proteins using FACS, western blots or microscopy (**Table 8**) as previously discussed above. The

positive and negative controls for each characterization experiment are outlined below (**Table 8**).

A potential problem of characterizing the deer mouse L-MVEC lies in the (commercially available) antibody's cross reactivity to the deer mouse L-MVEC because these antigens are derived from other mammalian species. If we continue to encounter this difficulty with any of the chosen antibodies, we will contact vendors for additional antibodies that are available. We have registered with AbCAM to provide them information on those we test, and to obtain other antibodies for the price of one.

During hantaviral infections SEOV showed the greatest increase of TGFβ which is promising because SEOV is more distantly related to SNV than is BCCV (which shows the second highest level). TGFβ has been shown to increase amounts NFκB through up-regulation of TNFα in human cervix epithelial (HeLa) cells and human lung epithelial (A549) cells [193]. Experiments conducted with SEOV in Norway rat macrophages showed an increase in TGFβ but not in L-MVEC [49]. It is very important to take into account that SNV was used to infect at a MOI ~20 fold less the MOI that was used for BCCV and SEOV. With that said SNV would have the highest level of TGFβ even if the fold change (Y-axis, **Figure 7**) was multiplied by a factor of 10 (half of the difference in MOI). Therefore, when taking into account the difference in MOI we can predict that infection of deer mouse L-MVEC with SNV, at a MOI of 1.0, is capable of mounting a TGFβ response as published in the literature for reservoir hantavirus infections.

Table 8.

L-MVEC characterization approach for FACS or Western Blots/Microscopy

Group	Receptors and Treatment		
	FACS		WB/M
	PECAM-1	ICAM-2	VE-Cadherin
Positive Control (Mouse or Deer mouse L-MVEC)	50 ng/mL VEGF [194, 195]	NA	NA
Negative Control (Mouse or Deer mouse L-MVEC)	TNFα (100 ng/mL) + INFγ (1000 U/mL) for 8 hr [194, 196, 197] or Trypsin EDTA treatment [191]	TNFα (10 ng/mL) + IL1β (34 ng/mL) for 24 hr [198]	ANDV MOI 1.0 for 24 hr [192]
Test (L-MVEC)	No treatment	No treatment	No treatment

We have shown that we can determine the titer of different hantaviruses using both plaque assay and cell-based ELISA. We were able to isolate viral RNA and monitor the expression levels of SNV and SEOV S-segment in deer mouse L-MVEC through qRT-PCR (SEOV data not shown). We have shown we are capable of isolating viral and cellular proteins from deer mouse infected L-MVEC. These techniques established in my preliminary data will be used in conjunction with each other for the future goals of my thesis.

The created primer set is effective for monitoring SNV S-segment replication (**Figure 12**). Further, we were also successfully able to isolate cellular proteins from infected deer mouse L-MVEC (**Figure 13**). In future experiments will use purified SNV N protein from Vero E6 cells as a positive control (to assess the primary antibody specificity and to quantify the amount of N protein being produced). We plan to keep calnexin as the loading control. Although, PFU/mL titers of BCCV and SEOV infected deer mouse supernatant had lost titer, the viruses were still detectable using cell-based ELISA ($TCID_{50}$/mL). The seed virus (veSNV) suggested a loss in titer, so we plan to regrow the virus seed and obtained another seed (**Table 7**). Lastly, the cell-based ELISA and plaque assay titers obtained for the Vero E6 derived viruses are not the same (**Table 7**). In future experiments we will quantify S-segment RNA and N protein amounts, which will give insight into which method is more accurate at determining the viral titer of our new *in vitro* deer mouse L-MVEC model.

Experiments conducted with SEOV in Norway rat macrophages showed an increase in TGFβ but not in L-MVEC [49]. In our experiments, SEOV showed

the greatest increase of TGFβ which is promising because SEOV is more distantly related to SNV than is BCCV (which shows the second highest level). TGFβ has been shown to increase amounts NFκB through up-regulation of TNFα in HeLa and A549 cells [193]. It is very important to take into account that SNV was used to infect at ~16 fold less than the MOI that was used for BCCV and SEOV. With that said SNV would have the highest level of TGFβ even if the level was only increased by a factor of 10.

Future Studies

The Hantavirus research community has little understanding regarding the adaptive steps that result in host switching of hantaviruses. My proposed future research aims to address this gap in knowledge using our novel, highly relevant *in vitro* L-MVEC model from the deer mouse. For future work, we aim to understand the viral determinants that allow persistence and the host responses that pose barriers to host adaptation. To achieve this, we plan to adapt the Old World SEOV to the deer mouse L-MVEC model. Adaptation will be monitored through viral titer, qRT-PCR of the S-segment and/or western blots of the N-protein.

Hantaviruses have mostly been isolated from wild rodents and rarely from human tissue using Vero E6 cells [113, 176, 177]. It is well established that RNA virus populations can undergo genetic changes from selective pressures in new host environments and a viruses fitness in one environment may not extended to a different environment, *in vitro* or *in vivo* [182-185]. This is shown for our viruses

in that SNV propagated in Vero E6 cells are unable to infect deer mouse L-MVEC, which is the site the virus has adapted to in nature (**Table 6**). Therefore, we plan to first "readapt" the viruses to their natural reservoir L-MVEC model, in order to have an isolate that resembles what is found in nature. We use the term "readapt" since our initial studies showed that Vero E6 propagated SNV showed a very low level of infection and hence, low fitness on deer mouse L-MVEC (**Table 7**).

We propose to examine the genetic architecture and fitness of the Vero E6 propagated SNV and SEOV (veSNV and veSEOV) versus seed stocks derived from reservoir L-MVEC deer mouse SNV (dmSNV) and Norway rat SEOV (nrSEOV) L-MVEC. To define the genetic architecture, we will measure the intrahost population richness by its genetic variability as determined by: (1) number of different mutations, (2) haplotype number, and/or (3) polymorphic variability of the entire genome. The diversity of the intra- and inter-host viral genome populations will be assessed using Shannon entropy, Simpson index and mutation frequency. We may also explore other approaches that are as yet unpublished. The sequences of SNV or SEOV isolates will be determined by Sanger Sequencing of the PCR product to obtain the consensus sequences and Ultra-deep pyrosequencing (UDPS). Sequences will be analyzed using Seq.Scape 2.1, Vector NTI, MEGA 5, the Shannon Entropy-Two calculator at Los Alamos (http://www.hiv.lanl.gov/content/sequence/ENTROPY/entropy. html), and the web based server Datamonkey.

Fitness of each virus will be determined by infecting Vero E6 or deer mouse L-MVEC in triplicate at a low 0.1, mid 0.5, and high 1.0 MOIs with each virus separately. The ability for each virus to replicate in each cell type will be determined by measurement of infectious particles ($TCID_{50}$/mL) released into supernatant at days 1, 2, 3, and 4 to measure viral titers (or alternatively PFU/mL). Viral titer will be plotted verses the day and the slope of the linear line of regression generated, will give the fitness of each virus [199].

After determining the differences between Vero E6 derived hantaviruses and "readapted" hantavirus, we will test the relationship of extrinsic (new host) pressures on preexisting intrahost genetic variation and viral fitness using *in vitro* models of adaptation (*spillover* and host-switching). To achieve this, we will use Norway rat adapted SEOV (nrSEOV) to adapt the virus to deer mouse L-MVEC (dm-nrSEOV). Adaptation of dm-nrSEOV will be monitored as above using qRT-PCR (S-segment), viral titer and N protein levels. We will use CCSS to determine the censuses sequence of our adapted viruses and UDPS to assess the genetic architecture and perform infections of Vero E6 and deer mouse L-MVEC to assess fitness. Lastly, in order to understand the host responses that pose barriers to host adaptation, we will characterize immune responses elicited in Vero E6 and deer mouse L-MVEC during infection with veSNV, veSEOV, dmSNV, nrSEOV, and dm-nrSEOV. The immune response will be assessed using qRT-PCR, using published primer sets (as discussed). We expect that viruses replicating in their reservoir will have high fitness and viruses replicating in their nonreservoir will have low fitness (**Table 9**). We expect the pro-

inflammatory immune response to be on during all Vero E6 infection and during nonreservoir infections of deer mouse L-MVEC (**Table 9**).

Conclusion

All data presented in **Chapter IV** is preliminary data characterizing the New World hantavirus (SNV-deer mouse L-MVEC) model for infection and has not been repeated. In establishing this model, we have successfully isolated and passaged L-MVEC cells from deer mice while maintaining ICAM-2 expression and consistent cell morphologies. We were able to see consistent L-MVEC morphologies over 8 passages without losing viability or proliferation (**Figure 10)**. After the initial isolation, ICAM-2 positive L-MVEC were selected using a magnetic bead secondary antibody (passage 2) (**Figure 10 A, B & C).** After further passaging of the L-MVEC to passages 4 and 8, we were able to maintain ICAM-2 expression and show consistent cell morphology over 8 passages (**Figure 10 D & E**).

Hantaviruses are known to be harbored by a single specific reservoir species for each isolate. The emergence of new hantavirus strains in nature is due to reassortment and spillover events that occur through rodent to rodent transmission of hantavirus. There have been limited studies on hantavirus spillover from their reservoir rodents into nonreservoir rodents, therefore little is known regarding how host restriction is overcome. The proposed study outlined in this chapter aims to address gap in our knowledge by adapting nonreservoir Old World, SEOV to a New World rodent reservoir (deer mouse L-MVEC).

Knowing which phenotypes are altered and assessing the immune response elicited during adaptation may provide insights into the host pathways that are manipulated or avoided by hantavirus during a reservoir infection.

Table 9

Proposed viruses and predicted phenotypes

Virus	Cell Line	Fitness Prediction	Innate Response Prediction	Level
veSNV	Vero E6	H	On	M
dmSNV	Vero E6	L	On	H
veSEOV	Vero E6	H	On	M
nrSEOV	Vero E6	L	On	H
dm-nrSEOV	Vero E6	L	On	H
veSNV	Deer mouse L-MVEC	L	On	H
dmSNV	Deer mouse L-MVEC	H	Off	L
veSEOV	Deer mouse L-MVEC	L	On	H
nrSEOV	Deer mouse L-MVEC	L	On	H
dm-nrSEOV	Deer mouse L-MVEC	H	Off	L

REFERENCES

1. **Lee, H.W., P.W. Lee, and K.M. Johnson, *Isolation of the etiologic agent of Korean hemorrhagic fever. 1978.* J Infect Dis, 1978. 137: p. 298-308.**
2. **Maher, J.F., *Trench nephritis: a retrospective perception.* Am J Kidney Dis, 1986. 7(5): p. 355-62.**
3. **Cameron, J.S., *The history of viral haemorrhagic fever with renal disease (hantavirus).* Nephrol. Dial. Transplant, 2001. 16: p. 1289-1290.**
4. **Myhrman, G., *Nephropathia epidemica a new infectious disease in northern Scandinavia.* Acta Med Scand, 1951. 140(1): p. 52-6.**
5. **Xiao, S.Y., et al., *Dobrava virus as a new Hantavirus: evidenced by comparative sequence analysis.* J Med Virol, 1993. 39(2): p. 152-5.**
6. **Klempa, B., et al., *Complex evolution and epidemiology of Dobrava-Belgrade hantavirus: definition of genotypes and their characteristics.* Arch Virol, 2013. 158(3): p. 521-9.**
7. **Lee, H.W., L.J. Baek, and K.M. Johnson, *Isolation of Hantaan virus, the etiologic agent of Korean hemorrhagic fever, from wild urban rats.* J Infect Dis, 1982. 146(5): p. 638-44.**
8. **Jonsson, C.B., L.T. Figueiredo, and O. Vapalahti, *A global perspective on hantavirus ecology, epidemiology, and disease.* Clin Microbiol Rev, 2010. 23(2): p. 412-41.**
9. **Lee, P.W., et al., *Partial characterization of Prospect Hill virus isolated from meadow voles in the United States.* J Infect Dis, 1985. 152(4): p. 826-9.**
10. **Tsai, T.F., et al., *Serological and virological evidence of a Hantaan virus-related enzootic in the United States.* J Infect Dis, 1985. 152(1): p. 126-36.**
11. **Weissenbacher, M.C., et al., *Hantavirus infection in laboratory and wild rodents in Argentina.* Medicina (B Aires), 1990. 50(1): p. 43-6.**
12. ***Update: outbreak of hantavirus infection--southwestern United States, 1993.* MMWR Morb Mortal Wkly Rep, 1993. 42(25): p. 495-6.**
13. **Nichol, S.T., et al., *Genetic identification of a hantavirus associated with an outbreak of acute respiratory illness.* Science, 1993. 262(5135): p. 914-7.**
14. **Hjelle, B., et al., *A novel hantavirus associated with an outbreak of fatal respiratory disease in the southwestern United States: evolutionary relationships to known hantaviruses.* J Virol, 1994. 68(2): p. 592-6.**
15. **Schmaljohn, C. and B. Hjelle, *Hantaviruses: a global disease problem.* Emerg Infect Dis, 1997. 3(2): p. 95-104.**
16. **Lopez, N., et al., *Genetic identification of a new hantavirus causing severe pulmonary syndrome in Argentina.* Virology, 1996. 220(1): p. 223-6.**
17. ***Hantavirus pulmonary syndrome -- Chile, 1997.* MMWR Morb Mortal Wkly Rep, 1997. 46(40): p. 949-51.**
18. **Toro, J., et al., *An outbreak of hantavirus pulmonary syndrome, Chile, 1997.* Emerg Infect Dis, 1998. 4(4): p. 687-94.**

19. Johnson, A.M., et al., *Laguna Negra virus associated with HPS in western Paraguay and Bolivia.* Virology, 1997. 238(1): p. 115-27.
20. Williams, R.J., et al., *An outbreak of hantavirus pulmonary syndrome in western Paraguay.* Am J Trop Med Hyg, 1997. 57(3): p. 274-82.
21. Pini, N., *Hantavirus pulmonary syndrome in Latin America.* Curr Opin Infect Dis, 2004. 17(5): p. 427-31.
22. Cantoni, G., et al., *Hantavirus pulmonary syndrome in the Province of Rio Negro, Argentina, 1993-1996.* Rev Inst Med Trop Sao Paulo, 1997. 39(4): p. 191-6.
23. Enria, D., et al., *Hantavirus pulmonary syndrome in Argentina. Possibility of person to person transmission.* Medicina (B Aires), 1996. 56(6): p. 709-11.
24. Padula, P.J., et al., *Hantavirus pulmonary syndrome outbreak in Argentina: molecular evidence for person-to-person transmission of Andes virus.* Virology, 1998. 241(2): p. 323-30.
25. Chaparro, J., et al., *Assessment of person-to-person transmission of hantavirus pulmonary syndrome in a Chilean hospital setting.* J Hosp Infect, 1998. 40(4): p. 281-5.
26. Ferres, M., et al., *Prospective evaluation of household contacts of persons with hantavirus cardiopulmonary syndrome in chile.* J Infect Dis, 2007. 195(11): p. 1563-71.
27. Schmaljohn, C.S. and J.M. Dalrymple, *Analysis of Hantaan virus RNA: evidence for a new genus of bunyaviridae.* Virology, 1983. 131(2): p. 482-91.
28. Jaaskelainen, K.M., et al., *Tula and Puumala hantavirus NSs ORFs are functional and the products inhibit activation of the interferon-beta promoter.* J Med Virol, 2007. 79(10): p. 1527-36.
29. Vera-Otarola, J., et al., *The Andes hantavirus NSs protein is expressed from the viral small mRNA by a leaky scanning mechanism.* J Virol, 2012. 86(4): p. 2176-87.
30. Elliot, R.M., *The Bunyaviridae, Concluding Remarks and Future Prospects*, in *The Bunyaviridae*, R.M. Elliot, Editor. 1996, Plenum Press: New York, London. p. 295-332.
31. Jonsson, C.B. and C.S. Schmaljohn, *Replication of hantaviruses.* Curr Top Microbiol Immunol, 2001. 256: p. 15-32.
32. Bouloy, M. and C. Hannoun, *Studies on lumbo virus replication. I. RNA-dependent RNA polymerase associated with virions.* Virology, 1976. 69(1): p. 258-64.
33. Hewlett, M.J., R.F. Pettersson, and D. Baltimore, *Circular forms of Uukuniemi virion RNA: an electron microscopic study.* J Virol, 1977. 21(3): p. 1085-93.
34. Battisti, A.J., et al., *Structural studies of Hantaan virus.* J Virol, 2011. 85(2): p. 835-41.
35. Huiskonen, J.T., et al., *Electron cryotomography of Tula hantavirus suggests a unique assembly paradigm for enveloped viruses.* J Virol, 2010. 84(10): p. 4889-97.
36. Flick, R. and R.F. Pettersson, *Reverse genetics system for Uukuniemi virus (Bunyaviridae): RNA polymerase I-catalyzed expression of chimeric viral RNAs.* J Virol, 2001. 75(4): p. 1643-55.
37. Flick, K., et al., *Functional analysis of the noncoding regions of the Uukuniemi virus (Bunyaviridae) RNA segments.* J Virol, 2004. 78(21): p. 11726-38.
38. Flick, R., et al., *Reverse genetics for crimean-congo hemorrhagic fever virus.* J Virol, 2003. 77(10): p. 5997-6006.
39. Billecocq, A., et al., *RNA polymerase I-mediated expression of viral RNA for the rescue of infectious virulent and avirulent Rift Valley fever viruses.* Virology, 2008. 378(2): p. 377-84.
40. Flick, K., et al., *Rescue of Hantaan virus minigenomes.* Virology, 2003. 306(2): p. 219-24.

41. Habjan, M., et al., *Processing of genome 5' termini as a strategy of negative-strand RNA viruses to avoid RIG-I-dependent interferon induction.* PLoS One, 2008. 3(4): p. e2032.
42. Lee, H.W. and H.J. Cho, *Electron microscope appearance of Hantaan virus, the causative agent of Korean haemorrhagic fever.* Lancet, 1981. 1(8229): p. 1070-2.
43. Gavrilovskaya, I.N., et al., *beta3 Integrins mediate the cellular entry of hantaviruses that cause respiratory failure.* Proc Natl Acad Sci U S A, 1998. 95(12): p. 7074-9.
44. Gavrilovskaya, I.N., et al., *Cellular entry of hantaviruses which cause hemorrhagic fever with renal syndrome is mediated by beta3 integrins.* J Virol, 1999. 73(5): p. 3951-9.
45. Krautkramer, E. and M. Zeier, *Hantavirus causing hemorrhagic fever with renal syndrome enters from the apical surface and requires decay-accelerating factor (DAF/CD55).* J Virol, 2008. 82(9): p. 4257-64.
46. Zaki, S.R., et al., *Hantavirus pulmonary syndrome. Pathogenesis of an emerging infectious disease.* Am J Pathol, 1995. 146(3): p. 552-79.
47. Raftery, M.J., et al., *Hantavirus infection of dendritic cells.* J Virol, 2002. 76(21): p. 10724-33.
48. Marsac, D., et al., *Infection of human monocyte-derived dendritic cells by ANDES Hantavirus enhances pro-inflammatory state, the secretion of active MMP-9 and indirectly enhances endothelial permeability.* Virol J, 2011. 8: p. 223.
49. Li, W. and S.L. Klein, *Seoul virus-infected rat lung endothelial cells and alveolar macrophages differ in their ability to support virus replication and induce regulatory T cell phenotypes.* J Virol, 2012. 86(21): p. 11845-55.
50. Jin, M., et al., *Hantaan virus enters cells by clathrin-dependent receptor-mediated endocytosis.* Virology, 2002. 294(1): p. 60-9.
51. Ramanathan, H.N. and C.B. Jonsson, *New and Old World hantaviruses differentially utilize host cytoskeletal components during their life cycles.* Virology, 2008. 374(1): p. 138-50.
52. Tischler, N.D., et al., *Hantavirus Gc glycoprotein: evidence for a class II fusion protein.* J Gen Virol, 2005. 86(Pt 11): p. 2937-47.
53. Cifuentes-Munoz, N., et al., *Aromatic and polar residues spanning the candidate fusion peptide of the Andes virus Gc protein are essential for membrane fusion and infection.* J Gen Virol, 2011. 92(Pt 3): p. 552-63.
54. Garcin, D., et al., *The 5' ends of Hantaan virus (Bunyaviridae) RNAs suggest a prime-and-realign mechanism for the initiation of RNA synthesis.* J Virol, 1995. 69(9): p. 5754-62.
55. Mir, M.A., et al., *Storage of cellular 5' mRNA caps in P bodies for viral cap-snatching.* Proc Natl Acad Sci U S A, 2008. 105(49): p. 19294-9.
56. Virtanen, J.O., et al., *Tula hantavirus NSs protein accumulates in the perinuclear area in infected and transfected cells.* Arch Virol, 2010. 155(1): p. 117-21.
57. Alfadhli, A., et al., *Hantavirus nucleocapsid protein oligomerization.* J Virol, 2001. 75(4): p. 2019-23.
58. Mir, M.A. and A.T. Panganiban, *Trimeric hantavirus nucleocapsid protein binds specifically to the viral RNA panhandle.* J Virol, 2004. 78(15): p. 8281-8.
59. Strandin, T., et al., *The cytoplasmic tail of hantavirus Gn glycoprotein interacts with RNA.* Virology, 2011. 418(1): p. 12-20.

60. **Strandin, T., J. Hepojoki, and A. Vaheri, *Cytoplasmic tails of bunyavirus Gn glycoproteins-Could they act as matrix protein surrogates?* Virology, 2013. 437(2): p. 73-80.**
61. **Ramanathan, H.N., et al., *Dynein-dependent transport of the hantaan virus nucleocapsid protein to the endoplasmic reticulum-Golgi intermediate compartment.* J Virol, 2007. 81(16): p. 8634-47.**
62. **Spiropoulou, C.F., *Hantavirus maturation.* Curr Top Microbiol Immunol, 2001. 256: p. 33-46.**
63. **Ravkov, E.V., S.T. Nichol, and R.W. Compans, *Polarized entry and release in epithelial cells of Black Creek Canal virus, a New World hantavirus.* J Virol, 1997. 71(2): p. 1147-54.**
64. **Rowe, R.K., J.W. Suszko, and A. Pekosz, *Roles for the recycling endosome, Rab8, and Rab11 in hantavirus release from epithelial cells.* Virology, 2008. 382(2): p. 239-49.**
65. **Meyer, B.J. and C.S. Schmaljohn, *Persistent hantavirus infections: characteristics and mechanisms.* Trends Microbiol, 2000. 8(2): p. 61-7.**
66. **Alff, P.J., et al., *The pathogenic NY-1 hantavirus G1 cytoplasmic tail inhibits RIG-I- and TBK-1-directed interferon responses.* J Virol, 2006. 80(19): p. 9676-86.**
67. **Vaheri, A., et al., *Uncovering the mysteries of hantavirus infections.* Nat Rev Microbiol, 2013. 11(8): p. 539-50.**
68. **Gavrilovskaya, I., et al., *The Role of the Endothelium in HPS Pathogenesis and Potential Therapeutic Approaches.* Adv Virol, 2012. 2012: p. 467059.**
69. **Schonrich, G., et al., *Hantavirus-induced immunity in rodent reservoirs and humans.* Immunol Rev, 2008. 225: p. 163-89.**
70. **Taylor, S.L., et al., *Endothelial Cell Permeability during Hantavirus Infection Involves Factor XII-Dependent Increased Activation of the Kallikrein-Kinin System.* PLoS Pathog, 2013. 9(7): p. e1003470.**
71. **Mackow, E.R. and I.N. Gavrilovskaya, *Hantavirus regulation of endothelial cell functions.* Thromb Haemost, 2009. 102(6): p. 1030-41.**
72. **Kruger, D.H., G. Schonrich, and B. Klempa, *Human pathogenic hantaviruses and prevention of infection.* Hum Vaccin, 2011. 7(6): p. 685-93.**
73. **Terajima, M. and F.A. Ennis, *T cells and pathogenesis of hantavirus cardiopulmonary syndrome and hemorrhagic fever with renal syndrome.* Viruses, 2011. 3(7): p. 1059-73.**
74. **Terajima, M., et al., *Immune responses to Puumala virus infection and the pathogenesis of nephropathia epidemica.* Microbes Infect, 2004. 6(2): p. 238-45.**
75. **Levine, J.R., et al., *Antagonism of type I interferon responses by new world hantaviruses.* J Virol, 2010. 84(22): p. 11790-801.**
76. **Linderholm, M., et al., *Elevated plasma levels of tumor necrosis factor (TNF)-alpha, soluble TNF receptors, interleukin (IL)-6, and IL-10 in patients with hemorrhagic fever with renal syndrome.* J Infect Dis, 1996. 173(1): p. 38-43.**
77. **Borges, A.A., et al., *Role of mixed Th1 and Th2 serum cytokines on pathogenesis and prognosis of hantavirus pulmonary syndrome.* Microbes Infect, 2008. 10(10-11): p. 1150-7.**
78. **Korva, M., et al., *Viral load and immune response dynamics in patients with haemorrhagic fever with renal syndrome.* Clin Microbiol Infect, 2013. 19(8): p. E358-66.**
79. **Kilpatrick, E.D., et al., *Role of specific CD8+ T cells in the severity of a fulminant zoonotic viral hemorrhagic fever, hantavirus pulmonary syndrome.* J Immunol, 2004. 172(5): p. 3297-304.**

80. Lindgren, T., et al., *Longitudinal analysis of the human T cell response during acute hantavirus infection.* J Virol, 2011. 85(19): p. 10252-60.
81. Schountz, T., et al., *Kinetics of immune responses in deer mice experimentally infected with Sin Nombre virus.* J Virol, 2012. 86(18): p. 10015-27.
82. Easterbrook, J.D. and S.L. Klein, *Seoul virus enhances regulatory and reduces proinflammatory responses in male Norway rats.* J Med Virol, 2008. 80(7): p. 1308-18.
83. Ma, Y., et al., *HLA-A2 and B35 restricted hantaan virus nucleoprotein CD8+ T-cell epitope-specific immune response correlates with milder disease in hemorrhagic fever with renal syndrome.* PLoS Negl Trop Dis, 2013. 7(2): p. e2076.
84. Dohmae, K., M. Okabe, and Y. Nishimune, *Experimental transmission of hantavirus infection in laboratory rats.* J Infect Dis, 1994. 170(6): p. 1589-92.
85. Hammerbeck, C.D. and J.W. Hooper, *T cells are not required for pathogenesis in the Syrian hamster model of hantavirus pulmonary syndrome.* J Virol, 2011. 85(19): p. 9929-44.
86. Gupta, S., et al., *Hantavirus-infection confers resistance to cytotoxic lymphocyte-mediated apoptosis.* PLoS Pathog, 2013. 9(3): p. e1003272.
87. Araki, K., et al., *Hantavirus-specific CD8(+)-T-cell responses in newborn mice persistently infected with Hantaan virus.* J Virol, 2003. 77(15): p. 8408-17.
88. Taruishi, M., et al., *Analysis of the immune response of Hantaan virus nucleocapsid protein-specific CD8+ T cells in mice.* Virology, 2007. 365(2): p. 292-301.
89. Easterbrook, J.D., M.C. Zink, and S.L. Klein, *Regulatory T cells enhance persistence of the zoonotic pathogen Seoul virus in its reservoir host.* Proc Natl Acad Sci U S A, 2007. 104(39): p. 15502-7.
90. Easterbrook, J.D. and S.L. Klein, *Immunological mechanisms mediating hantavirus persistence in rodent reservoirs.* PLoS Pathog, 2008. 4(11): p. e1000172.
91. Schountz, T., et al., *Regulatory T cell-like responses in deer mice persistently infected with Sin Nombre virus.* Proc Natl Acad Sci U S A, 2007. 104(39): p. 15496-501.
92. Zhu, L.Y., et al., *Reduced circulating CD4+CD25+ cell populations in haemorrhagic fever with renal syndrome.* Clin Exp Immunol, 2009. 156(1): p. 88-96.
93. Belkaid, Y., *Regulatory T cells and infection: a dangerous necessity.* Nat Rev Immunol, 2007. 7(11): p. 875-88.
94. Au, R.Y., et al., *Seoul virus suppresses NF-kappaB-mediated inflammatory responses of antigen presenting cells from Norway rats.* Virology, 2010. 400(1): p. 115-27.
95. Erickson, J.J., et al., *Viral acute lower respiratory infections impair CD8+ T cells through PD-1.* J Clin Invest, 2012. 122(8): p. 2967-82.
96. Gianchecchi, E., D.V. Delfino, and A. Fierabracci, *Recent insights into the role of the PD-1/PD-L1 pathway in immunological tolerance and autoimmunity.* Autoimmun Rev, 2013. 12(11): p. 1091-100.
97. Watanabe, T., A. Bertoletti, and T.A. Tanoto, *PD-1/PD-L1 pathway and T-cell exhaustion in chronic hepatitis virus infection.* J Viral Hepat, 2010. 17(7): p. 453-8.
98. Rang, A., *Modulation of innate immune responses by hantaviruses.* Crit Rev Immunol, 2010. 30(6): p. 515-27.
99. Matthys, V. and E.R. Mackow, *Hantavirus regulation of type I interferon responses.* Adv Virol, 2012. 2012: p. 524024.
100. Klingstrom, J. and C. Ahlm, *Hantavirus protein interactions regulate cellular functions and signaling responses.* Expert Rev Anti Infect Ther, 2011. 9(1): p. 33-47.

101. **Spiropoulou, C.F., et al.,** ***Andes and Prospect Hill hantaviruses differ in early induction of interferon although both can downregulate interferon signaling.*** **J Virol, 2007. 81(6): p. 2769-76.**

102. **Alff, P.J., et al.,** ***The NY-1 hantavirus Gn cytoplasmic tail coprecipitates TRAF3 and inhibits cellular interferon responses by disrupting TBK1-TRAF3 complex formation.*** **J Virol, 2008. 82(18): p. 9115-22.**

103. **Stoltz, M. and J. Klingstrom,** ***Alpha/beta interferon (IFN-alpha/beta)-independent induction of IFN-lambda1 (interleukin-29) in response to Hantaan virus infection.*** **J Virol, 2010. 84(18): p. 9140-8.**

104. **Taylor, S.L., et al.,** ***Hantaan virus nucleocapsid protein binds to importin alpha proteins and inhibits tumor necrosis factor alpha-induced activation of nuclear factor kappa B.*** **J Virol, 2009. 83(3): p. 1271-9.**

105. **Backes, C., et al.,** ***GraBCas: a bioinformatics tool for score-based prediction of Caspase- and Granzyme B-cleavage sites in protein sequences.*** **Nucleic Acids Res, 2005. 33(Web Server issue): p. W208-13.**

106. **Ontiveros, S.J., Q. Li, and C.B. Jonsson,** ***Modulation of apoptosis and immune signaling pathways by the Hantaan virus nucleocapsid protein.*** **Virology, 2010. 401(2): p. 165-78.**

107. **Taylor, S.L., R.L. Krempel, and C.S. Schmaljohn,** ***Inhibition of TNF-alpha-induced activation of NF-kappaB by hantavirus nucleocapsid proteins.*** **Ann N Y Acad Sci, 2009. 1171 Suppl 1: p. E86-93.**

108. **Kang, H.J., et al.,** ***Host switch during evolution of a genetically distinct hantavirus in the American shrew mole (Neurotrichus gibbsii).*** **Virology, 2009. 388(1): p. 8-14.**

109. **Kang, H.J., et al.,** ***Evolutionary insights from a genetically divergent hantavirus harbored by the European common mole (Talpa europaea).*** **PLoS One, 2009. 4(7): p. e6149.**

110. **Arai, S., et al.,** ***Molecular phylogeny of a newfound hantavirus in the Japanese shrew mole (Urotrichus talpoides).*** **Proc Natl Acad Sci U S A, 2008. 105(42): p. 16296-301.**

111. **Guo, W.P., et al.,** ***Phylogeny and origins of hantaviruses harbored by bats, insectivores, and rodents.*** **PLoS Pathog, 2013. 9(2): p. e1003159.**

112. **Severson, W.E., et al.,** ***Ribavirin causes error catastrophe during Hantaan virus replication.*** **J Virol, 2003. 77(1): p. 481-8.**

113. **Vapalahti, O., et al.,** ***Isolation and characterization of a hantavirus from Lemmus sibiricus: evidence for host switch during hantavirus evolution.*** **J Virol, 1999. 73(7): p. 5586-92.**

114. **Sibold, C., et al.,** ***Recombination in Tula hantavirus evolution: analysis of genetic lineages from Slovakia.*** **J Virol, 1999. 73(1): p. 667-75.**

115. **Morse, S.S.,** ***Factors in the emergence of infectious diseases.*** **Emerg Infect Dis, 1995. 1(1): p. 7-15.**

116. **Both, G.W., et al.,** ***Antigenic drift in influenza virus H3 hemagglutinin from 1968 to 1980: multiple evolutionary pathways and sequential amino acid changes at key antigenic sites.*** **J Virol, 1983. 48(1): p. 52-60.**

117. **Vapalahti, O., et al.,** ***Human B-cell epitopes of Puumala virus nucleocapsid protein, the major antigen in early serological response.*** **J Med Virol, 1995. 46(4): p. 293-303.**

118. **Novella, I.S., et al.,** ***Congruent evolution of fitness and genetic robustness in vesicular stomatitis virus.*** **J Virol, 2013. 87(9): p. 4923-8.**

119. **Delport, W., et al.,** ***Datamonkey 2010: a suite of phylogenetic analysis tools for evolutionary biology.*** **Bioinformatics, 2010. 26(19): p. 2455-7.**

120. Pond, S.L. and S.D. Frost, *Datamonkey: rapid detection of selective pressure on individual sites of codon alignments.* Bioinformatics, 2005. 21(10): p. 2531-3.
121. Pond, S.L. and S.D. Frost, *A genetic algorithm approach to detecting lineage-specific variation in selection pressure.* Mol Biol Evol, 2005. 22(3): p. 478-85.
122. Botten, J., et al., *Shedding and intracage transmission of Sin Nombre hantavirus in the deer mouse (Peromyscus maniculatus) model.* J Virol, 2002. 76(15): p. 7587-94.
123. Ebihara, H., et al., *Pathogenicity of Hantaan virus in newborn mice: genetic reassortant study demonstrating that a single amino acid change in glycoprotein G1 is related to virulence.* J Virol, 2000. 74(19): p. 9245-55.
124. Hutchinson, K.L., P.E. Rollin, and C.J. Peters, *Pathogenesis of a North American hantavirus, Black Creek Canal virus, in experimentally infected Sigmodon hispidus.* Am J Trop Med Hyg, 1998. 59(1): p. 58-65.
125. Lokugamage, K., et al., *Comparison of virulence of various hantaviruses related to hemorrhagic fever with renal syndrome in newborn mouse model.* Jpn J Vet Res, 2004. 51(3-4): p. 143-9.
126. Hooper, J.W., et al., *Hantaan/Andes virus DNA vaccine elicits a broadly cross-reactive neutralizing antibody response in nonhuman primates.* Virology, 2006. 347(1): p. 208-16.
127. Hooper, J.W., et al., *A lethal disease model for hantavirus pulmonary syndrome.* Virology, 2001. 289(1): p. 6-14.
128. Huggins, J.W., et al., *Prospective, double-blind, concurrent, placebo-controlled clinical trial of intravenous ribavirin therapy of hemorrhagic fever with renal syndrome.* J Infect Dis, 1991. 164(6): p. 1119-27.
129. Huggins, J.W., et al., *Ribavirin therapy for Hantaan virus infection in suckling mice.* J Infect Dis, 1986. 153(3): p. 489-97.
130. Rusnak, J.M., et al., *Experience with intravenous ribavirin in the treatment of hemorrhagic fever with renal syndrome in Korea.* Antiviral Res, 2009. 81(1): p. 68-76.
131. Safronetz, D., et al., *The Syrian hamster model of hantavirus pulmonary syndrome.* Antiviral Res, 2012. 95(3): p. 282-92.
132. Bull, J.J., R. Sanjuan, and C.O. Wilke, *Theory of lethal mutagenesis for viruses.* J Virol, 2007. 81(6): p. 2930-9.
133. Daifuku, R., *Stealth nucleosides: mode of action and potential use in the treatment of viral diseases.* BioDrugs, 2003. 17(3): p. 169-77.
134. Freistadt, M.S., G.D. Meades, and C.E. Cameron, *Lethal mutagens: broad-spectrum antivirals with limited potential for development of resistance?* Drug Resist Updat, 2004. 7(1): p. 19-24.
135. Jonsson, C.B., B.G. Milligan, and J.B. Arterburn, *Potential importance of error catastrophe to the development of antiviral strategies for hantaviruses.* Virus Res, 2005. 107(2): p. 195-205.
136. Graci, J.D. and C.E. Cameron, *Mechanisms of action of ribavirin against distinct viruses.* Rev Med Virol, 2006. 16(1): p. 37-48.
137. Leyssen, P., et al., *The predominant mechanism by which ribavirin exerts its antiviral activity in vitro against flaviviruses and paramyxoviruses is mediated by inhibition of IMP dehydrogenase.* J Virol, 2005. 79(3): p. 1943-7.
138. Malinoski, F. and V. Stollar, *Inhibitors of IMP dehydrogenase prevent sindbis virus replication and reduce GTP levels in Aedes albopictus cells.* Virology, 1981. 110(2): p. 281-9.

139. **Goswami, B.B., et al., *The broad spectrum antiviral agent ribavirin inhibits capping of mRNA.* Biochem Biophys Res Commun, 1979. 89(3): p. 830-6.**

140. **Toltzis, P. and A.S. Huang, *Effect of ribavirin on macromolecular synthesis in vesicular stomatitis virus-infected cells.* Antimicrob Agents Chemother, 1986. 29(6): p. 1010-6.**

141. **Eriksson, B., et al., *Inhibition of influenza virus ribonucleic acid polymerase by ribavirin triphosphate.* Antimicrob Agents Chemother, 1977. 11(6): p. 946-51.**

142. **Fernandez-Larsson, R., et al., *Molecular analysis of the inhibitory effect of phosphorylated ribavirin on the vesicular stomatitis virus in vitro polymerase reaction.* Antimicrob Agents Chemother, 1989. 33(10): p. 1668-73.**

143. **Wray, S.K., B.E. Gilbert, and V. Knight, *Effect of ribavirin triphosphate on primer generation and elongation during influenza virus transcription in vitro.* Antiviral Res, 1985. 5(1): p. 39-48.**

144. **Crotty, S., C. Cameron, and R. Andino, *Ribavirin's antiviral mechanism of action: lethal mutagenesis?* J Mol Med (Berl), 2002. 80(2): p. 86-95.**

145. **Crotty, S., C.E. Cameron, and R. Andino, *RNA virus error catastrophe: direct molecular test by using ribavirin.* Proc Natl Acad Sci U S A, 2001. 98(12): p. 6895-900.**

146. **Cuevas, J.M., et al., *Effect of ribavirin on the mutation rate and spectrum of hepatitis C virus in vivo.* J Virol, 2009. 83(11): p. 5760-4.**

147. **Vignuzzi, M., J.K. Stone, and R. Andino, *Ribavirin and lethal mutagenesis of poliovirus: molecular mechanisms, resistance and biological implications.* Virus Res, 2005. 107(2): p. 173-81.**

148. **Tam, R.C., et al., *Ribavirin polarizes human T cell responses towards a Type 1 cytokine profile.* J Hepatol, 1999. 30(3): p. 376-82.**

149. **Kobayashi, T., et al., *Ribavirin modulates the conversion of human CD4(+) CD25(-) T cell to CD4(+) CD25(+) FOXP3(+) T cell via suppressing interleukin-10-producing regulatory T cell.* Immunology, 2012. 137(3): p. 259-70.**

150. **Sun, Y., et al., *Activity of ribavirin against Hantaan virus correlates with production of ribavirin-5'-triphosphate, not with inhibition of IMP dehydrogenase.* Antimicrob Agents Chemother, 2007. 51(1): p. 84-8.**

151. **Chung, D.H., et al., *Ribavirin reveals a lethal threshold of allowable mutation frequency for Hantaan virus.* J Virol, 2007. 81(21): p. 11722-9.**

152. **Severson, W.E., et al., *Ribavirin causes error catastrophe during Hantaan virus replication.* J Virol., 2003. 77(1): p. 481-8.**

153. **Takenaka, A., C.J. Gibbs, Jr., and D.C. Gajdusek, *Antiviral neutralizing antibody to Hantaan virus as determined by plaque reduction technique.* Arch Virol, 1985. 84(3-4): p. 197-206.**

154. **Tamura, K., et al., *MEGA5: molecular evolutionary genetics analysis using maximum likelihood, evolutionary distance, and maximum parsimony methods.* Mol Biol Evol, 2011. 28(10): p. 2731-9.**

155. **Schmaljohn, C.S., et al., *Coding strategy of the S genome segment of Hantaan virus.* Virology, 1986. 155(2): p. 633-43.**

156. **Chung, D.H., et al., *Synthesis of 1-beta-D-ribofuranosyl-3-ethynyl-[1,2,4]triazole and its in vitro and in vivo efficacy against Hantavirus.* Antiviral Res, 2008. 79(1): p. 19-27.**

157. **Tamura, K. and M. Nei, *Estimation of the number of nucleotide substitutions in the control region of mitochondrial DNA in humans and chimpanzees.* Mol Biol Evol, 1993. 10(3): p. 512-26.**

158. Kosakovsky Pond, S.L. and S.D. Frost, *Not so different after all: a comparison of methods for detecting amino acid sites under selection.* Mol Biol Evol, 2005. 22(5): p. 1208-22.
159. Murrell, B., et al., *Detecting individual sites subject to episodic diversifying selection.* PLoS Genet, 2012. 8(7): p. e1002764.
160. Peters, C.J., G.L. Simpson, and H. Levy, *Spectrum of hantavirus infection: hemorrhagic fever with renal syndrome and hantavirus pulmonary syndrome.* Annu Rev Med, 1999. 50: p. 531-45.
161. Chapman, L.E., et al., *Intravenous ribavirin for hantavirus pulmonary syndrome: safety and tolerance during 1 year of open-label experience. Ribavirin Study Group.* Antivir Ther, 1999. 4(4): p. 211-9.
162. Mertz, G.J., et al., *Placebo-controlled, double-blind trial of intravenous ribavirin for the treatment of hantavirus cardiopulmonary syndrome in North America.* Clin Infect Dis, 2004. 39(9): p. 1307-13.
163. Safronetz, D., et al., *In vitro and in vivo activity of ribavirin against Andes virus infection.* PLoS One, 2011. 6(8): p. e23560.
164. Anderson, J.P., R. Daifuku, and L.A. Loeb, *Viral error catastrophe by mutagenic nucleosides.* Annu Rev Microbiol, 2004. 58: p. 183-205.
165. Crotty, S., et al., *The broad-spectrum antiviral ribonucleoside ribavirin is an RNA virus mutagen.* Nat Med, 2000. 6(12): p. 1375-9.
166. Graci, J.D. and C.E. Cameron, *Quasispecies, error catastrophe, and the antiviral activity of ribavirin.* Virology, 2002. 298(2): p. 175-80.
167. Tam, R.C., J.Y. Lau, and Z. Hong, *Mechanisms of action of ribavirin in antiviral therapies.* Antivir Chem Chemother, 2001. 12(5): p. 261-72.
168. Sanz-Ramos, M., T. Rodriguez-Calvo, and N. Sevilla, *Mutagenesis-mediated decrease of pathogenicity as a feature of the mutant spectrum of a viral population.* PLoS One, 2012. 7(6): p. e39941.
169. Graci, J.D., et al., *Mutational robustness of an RNA virus influences sensitivity to lethal mutagenesis.* J Virol, 2012. 86(5): p. 2869-73.
170. Li, X.D., et al., *Hantavirus nucleocapsid protein interacts with the Fas-mediated apoptosis enhancer Daxx.* J Gen Virol, 2002. 83(Pt 4): p. 759-66.
171. Kaukinen, P., A. Vaheri, and A. Plyusnin, *Non-covalent interaction between nucleocapsid protein of Tula hantavirus and small ubiquitin-related modifier-1, SUMO-1.* Virus Res, 2003. 92(1): p. 37-45.
172. Song, G., *Epidemiological progresses of hemorrhagic fever with renal syndrome in China.* Chin Med J (Engl), 1999. 112(5): p. 472-7.
173. Hughes, A.L. and R. Friedman, *Evolutionary diversification of protein-coding genes of hantaviruses.* Mol Biol Evol, 2000. 17(10): p. 1558-68.
174. Sironen, T., A. Vaheri, and A. Plyusnin, *Molecular evolution of Puumala hantavirus.* J Virol, 2001. 75(23): p. 11803-10.
175. Plyusnin, A. and S.P. Morzunov, *Virus evolution and genetic diversity of hantaviruses and their rodent hosts.* Curr Top Microbiol Immunol, 2001. 256: p. 47-75.
176. Schmaljohn, A.L., et al., *Isolation and initial characterization of a newfound hantavirus from California.* Virology, 1995. 206(2): p. 963-72.
177. Lee, H.W., P.W. Lee, and K.M. Johnson, *Isolation of the etiologic agent of Korean hemorrhagic fever. 1978.* J Infect Dis, 2004. 190(9): p. 1711-21.
178. Stoltz, M., et al., *A model system for in vitro studies of bank vole borne viruses.* PLoS One, 2011. 6(12): p. e28992.

179. Chung, D.H., et al., *The murine model for Hantaan virus-induced lethal disease shows two distinct paths in viral evolutionary trajectory with and without ribavirin treatment.* J Virol, 2013. 87(20): p. 10997-1007.
180. Ravkov, E.V. and R.W. Compans, *Hantavirus nucleocapsid protein is expressed as a membrane-associated protein in the perinuclear region.* J Virol, 2001. 75(4): p. 1808-15.
181. McElroy, A.K., et al., *Andes virus infection of cynomolgus macaques.* J Infect Dis, 2002. 186(12): p. 1706-12.
182. Holland, J.J., et al., *Quantitation of relative fitness and great adaptability of clonal populations of RNA viruses.* J Virol, 1991. 65(6): p. 2960-7.
183. Turner, P.E. and S.F. Elena, *Cost of host radiation in an RNA virus.* Genetics, 2000. 156(4): p. 1465-70.
184. Nemirov, K., et al., *Adaptation of Puumala hantavirus to cell culture is associated with point mutations in the coding region of the L segment and in the noncoding regions of the S segment.* J Virol, 2003. 77(16): p. 8793-800.
185. Lundkvist, A., et al., *Cell culture adaptation of Puumala hantavirus changes the infectivity for its natural reservoir, Clethrionomys glareolus, and leads to accumulation of mutants with altered genomic RNA S segment.* J Virol, 1997. 71(12): p. 9515-23.
186. Schountz, T., et al., *Expression profiling of lymph node cells from deer mice infected with Andes virus.* BMC Immunol, 2013. 14(1): p. 18.
187. Hartwell, D.W., et al., *Role of P-selectin cytoplasmic domain in granular targeting in vivo and in early inflammatory responses.* J Cell Biol, 1998. 143(4): p. 1129-41.
188. Lee, H.W., C.H. Calisher, and C.S. Schmaljohn, *Manual of hemorrhagic fever with renal syndrome and hantavirus pulmonary syndrome*. 1998: WHO Collaborating Center for Virus Reference and Research (Hantaviruses).
189. Fehrenbach, M.L., et al., *Isolation of murine lung endothelial cells.* Am J Physiol Lung Cell Mol Physiol, 2009. 296(6): p. L1096-103.
190. Schniedermann, J., et al., *Mouse lung contains endothelial progenitors with high capacity to form blood and lymphatic vessels.* BMC Cell Biol, 2010. 11: p. 50.
191. Marelli-Berg, F.M., et al., *Isolation of endothelial cells from murine tissue.* J Immunol Methods, 2000. 244(1-2): p. 205-15.
192. Shrivastava-Ranjan, P., P.E. Rollin, and C.F. Spiropoulou, *Andes virus disrupts the endothelial cell barrier by induction of vascular endothelial growth factor and downregulation of VE-cadherin.* J Virol, 2010. 84(21): p. 11227-34.
193. Ishinaga, H., et al., *Synergistic induction of nuclear factor-kappaB by transforming growth factor-beta and tumour necrosis factor-alpha is mediated by protein kinase A-dependent RelA acetylation.* Biochem J, 2009. 417(2): p. 583-91.
194. Woodfin, A., M.B. Voisin, and S. Nourshargh, *PECAM-1: a multi-functional molecule in inflammation and vascular biology.* Arterioscler Thromb Vasc Biol, 2007. 27(12): p. 2514-23.
195. Esser, S., et al., *Vascular endothelial growth factor induces VE-cadherin tyrosine phosphorylation in endothelial cells.* J Cell Sci, 1998. 111 (Pt 13): p. 1853-65.
196. Stewart, R.J., T.S. Kashour, and P.A. Marsden, *Vascular endothelial platelet endothelial adhesion molecule-1 (PECAM-1) expression is decreased by TNF-alpha and IFN-gamma. Evidence for cytokine-induced destabilization of messenger ribonucleic acid transcripts in bovine endothelial cells.* J Immunol, 1996. 156(3): p. 1221-8.

197. **Rival, Y., et al.,** ***Inhibition of platelet endothelial cell adhesion molecule-1 synthesis and leukocyte transmigration in endothelial cells by the combined action of TNF-alpha and IFN-gamma.*** **J Immunol, 1996. 157(3): p. 1233-41.**

198. **McLaughlin, F., et al.,** ***Tumor necrosis factor (TNF)-alpha and interleukin (IL)-1beta down-regulate intercellular adhesion molecule (ICAM)-2 expression on the endothelium.*** **Cell Adhes Commun, 1998. 6(5): p. 381-400.**

199. **Maree, A.F., et al.,** ***Estimating relative fitness in viral competition experiments.*** **J Virol, 2000. 74(23): p. 11067-72.**

Appendix A

LIST OF ABBREVIATIONS

Hantaan Virus	.....	HTNV
Hemorrhagic Fever with Renal Syndrome	.....	HFRS
Nephropathia epidemica	.....	NE
Dobrava-Belgrade virus	.....	DOBV
Seoul virus	.....	SEOV
Puumala virus	.....	PUUV
Prospect Hill virus	.....	PHV
Hantavirus Pulmonary Syndrome	.....	HPS
Adult respiratory Distress Syndrome	.....	ARDS
Office of the Medical Investigator	.....	OMI
Center for Disease Control	.....	CDC
Sin Nombre virus	.....	SNV
Andes virus	.....	ANDV
Laguna-Negra virus	.....	LANV
Small	.....	S
Medium	.....	M
Large	.....	L
Nucleocapsid	.....	N
Glycoproteins	.....	G_N/G_C
RNA dependent Reverse polymerase	.....	RdRp
Nonstructural Protein	.....	NSs
Viral RNA	.....	vRNA
Complementary RNA	.....	cRNA
Messenger RNA	.....	mRNA
Ribonucleoprotein	.....	RNP
Cryoelectron Microscopy	.....	Cryo-EM
Tula virus	.....	TULV
Rough Endoplasmic Reticulum	.....	RER
ER-Golgi Intermediate Complex	.....	ERGIC
Black Creek Canal virus	.....	BCCV
Vascular endothelial growth factor	.....	VEGF
Bradykinin	.....	BK
Cytotoxic T Lymphocytes	.....	CTL
Days post infection	.....	dpi
Peripheral blood mononuclear cells	.....	PBMC
Protein Dependent Ligand 1	.....	PD-L1
Major histocompatibility complex	.....	MHC
Regulatory T cells	.....	Treg
Foxhead box	.....	Fox
T Helper cells	.....	T_H1 or T_H2
Antigen Presenting Cell	.....	APC
Nuclear Factor Kappa-B	.....	NFkB
Human immunodeficiency virus	.....	HIV

Hepatitis B virus	.....	HBV
Hepatitis C virus	.....	HCV
glycoproteins	.....	GPCs
New York virus	.....	NYV
IFN sequence regulatory element	.....	ISRE
Natural Killer	.....	NK
Food and Drug Administration	.....	FDA
Interferon	.....	IFN
Antigenic Drift	.....	AGD
Antigenic Shift	.....	AGS
reproductive value	.....	R_0
Genetic Selective Sweep	.....	GSS
Nonsynonymous Error rate	.....	(*dN*)
Synonymous Error rate	.....	(*dS*)
Single-Likelihood Ancestor Counting	.....	SLAC
Fixed-Effects Likelihood	.....	FEL
Internal Fixed-Effects Likelihood	.....	iFEL
Mixed-Effects Model of Evolution	.....	MEM
Fast Unbiased Bayesian Approximation	.....	FUBAR
((*dN*) / (*dS*)) ratio	.....	ω
Inosine Monophosphate Dehydrogenase	.....	IMPDH
Plaque Forming Units	.....	PFU
Days postnatal	.....	dpn
Dulbecco's Modified Eagles Medium	.....	DMEM
Fetal Bovine Serum		FBS
Institutional Animal Care and Use Committee	.....	IACUC
Intracranial	.....	i.c.
Reverse Transcriptase	.....	RT
Nucleotides	.....	nt
Generalized Linear Models	.....	GLM
Akaike Information Criterion	.....	AIC
Mean Time to Death	.....	MTD
Analysis of Variance	.....	ANOVA
Selective Infectivity	.....	PFU/vRNA
Amino Acid	.....	aa
Foot-and-Mouth disease virus	.....	FMDV
International Committee on Taxonomy of Viruses	.....	ICTV
Lung Microvascular Endothelial cells	.....	L-MVEC
Convict Creek 107	.....	CC107
National Institute of Health	.....	NIH
Clinical Translational Research Building	.....	CTRB
Complete Endothelial Cell Culture Media	.....	M1168
Dulbecco's phosphate-buffered saline		DPBS
Facilitated-Activated Cell Sorting	.....	FACS
Sodium Dodecyl Sulfate	.....	SDS

Polyacrylamide Gel Electrophoresis	……...	PAGE
Horseradish Peroxidase	……...	HRP
2,2'-Azino bis [3-ethylbenzothiazoline-6-sulfonic acid]-diammonium salt	……...	ABTS
Glyceraldehyde-3-phosphate Dehydrogenase	……...	GAPDH
Minimal Essential Medium		MEM
Roswell Park Memorial Institute		RPMI
Vero E6 propagated SNV	……...	veSNV
Western Blot	……...	WB
Vero E6 propagated SEOV	……...	veSEOV
Vero E6 propagated BCCV	……...	veBCCV
hours post infection	……...	hpi
TNFα-receptor-mediated-signaling	……...	TNFR
human cervix epithelial cells	……...	HeLa
human lung epithelial cell line	……...	A549
deer mouse L-MVEC SNV	……...	dmSNV
Norway rat L-MVEC SEOV	……...	nrSEOV
Conventional Cloning Sanger Sequencing	……...	CCSS
Ultra-Deep Pyrosequencing	……...	UDPS
deer mouse L-MVEC adapted nr-SEOV	……...	dm-nrSEOV

Appendix B

Permission to use Future Medicine Ltd copyright material

Request from:

- Contact name: Ryan McAllister
- Publisher/company name: University of Louisville
- Address:
- Telephone/e-mail: Rcmcal01@louisville.edu

Request details:

- Request to use the following content: Full text - Future Virology, January 2014, Vol. 9, No. 1, Pages 87-99
- In the following publication: As part of the First Chapter for both his thesis and dissertation.
- In what media (print/electronic/print & electronic): Print and Electronic
- In the following languages: All

We, Future Medicine Ltd, grant permission to reuse the material specified above within the publication specified above.

Notes and conditions:

1. This permission is granted free of charge, for one-time use only.
2. Future Medicine Ltd grant the publisher non-exclusive world rights to publish the content in the publication/website specified above.
3. Future Medicine Ltd retains copyright ownership of the content.
4. Permission is granted on a one-time basis only. Separate permission is required for any further use or edition.
5. The publisher will make due acknowledgement of the original publication wherever they republish the content: citing the author, content title, publication name and Future Medicine Ltd as the original publisher.
6. The publisher will not amend, abridge, or otherwise change the content without authorization from Future Medicine Ltd.
7. Permission does not include any copyrighted material from other sources that may be incorporated within the content.
8. Failure to comply with the conditions above will result in immediate revocation of the permission here granted.

Date: 09/04/2014

Future Medicine Ltd, Unitec House, 2 Albert Place, London, N3 1QB, UK
T: +44 (0)20 8371 6080 F: +44 (0) 20 8371 6099 E: info@futuremedicine.com
www.futuremedicine.com

Appendix C

RightsLink®

Home | Create Account | Help

AMERICAN SOCIETY FOR MICROBIOLOGY

Title: The Murine Model for Hantaan virus-Induced Lethal Disease Shows Two Distinct Paths in Viral Evolutionary Trajectory with or without Ribavirin Treatment

Author: Dong-Hoon Chung, Åke Västermark, Jeremy V. Camp et al.

Publication: Journal of Virology

Publisher: American Society for Microbiology

Date: Jul 31, 2013

User ID

Password

Enable Auto Login

LOGIN

Forgot Password/User ID?

If you're a copyright.com user, you can login to RightsLink using your copyright.com credentials. Already **a RightsLink user** or want to learn more?

Permissions Request

Authors in ASM journals retain the right to republish discrete portions of his/her article in any other publication (including print, CD-ROM, and other electronic formats) of which he or she is author or editor, provided that proper credit is given to the original ASM publication. ASM authors also retain the right to reuse the full article in his/her dissertation or thesis. For a full list of author rights, please see: http://journals.asm.org/site/misc/ASM_Author_Statement.xhtml

BACK | CLOSE WINDOW

CURRICULUM VITA

Name :	Ryan Carroll McAllister
Address:	Center for Predictive Medicine CTRB 505 S. Hancock St. 626 Louisville, KY 40202
DOB:	Detroit, Michigan - April 3, 1988
Education & Training:	B.S., Biochemistry Northern Michigan University Current Graduate Student at University of Louisville under Colleen Jonsson
Extracurricular Activities	Northern Michigan University Football Player Organic Chemistry Tutor (Northern Michigan University)
Awards:	IPIBS
Professional Societies:	American Society for Virology member 2013 and 2014
Publications:	Camp, J.V., et al., *Phenotypic differences in virulence and immune response in closely related clinical isolates of influenza A 2009 H1N1 pandemic viruses in mice.* PLoS One, 2013. **8**(2): p. e56602. Chung, D.H., et al., *The Murine Model for Hantaan Virus-Induced Lethal Disease Shows Two Distinct Paths in Viral Evolutionary Trajectory with and without Ribavirin Treatment.* J Virol, 2013. 87(20): p. 10997-1007. Ryan C McAllister and Colleen B Jonsson. *Hantaviruses: past, present and future.* Future Virology 2014 9:1, 87-99.